MSc Research

Evaluating vegetation regeneration rates after drought

Niek Geelen, 6538169

Utrecht University
Department of Physical Geography
The Netherlands
31/01/24

Utrecht University

1st Supervisor: Dr. Ir. Niko Wanders
2nd Supervisor: Jennie C. Steyaert

Abstract

Drought events have accelerated and intensified in recent decades. In the 21st century, the number and duration of severe drought events are expected to increase even further. The impact on crops and natural vegetation has already become more pronounced over the last years, as crop yield losses increase and forest fires become more frequent. This creates increasing pressure on water demand and food security globally. Therefore, it is important to understand not only the impact of droughts on vegetation but also the regeneration of vegetation in post-drought periods. In this study, vegetation regeneration rates in Nebraska (United States) are determined using the Standardized Precipitation Evapotranspiration Index (SPEI) and the Enhanced Vegetation Index (EVI). The results show that the correlation coefficient between the SPEI and EVI is generally high for grassland (0.8 - 1.0) and low for cropland ($\sim$ 0.2). The time shift, days between the two datasets at the highest possible correlation coefficient, is between 75 and 125 days for grassland which is mainly dependent on the local topography which is the main driver of groundwater flow and therefore hydraulic gradients in the area. Various factors, including the water table, rooting depth, groundwater recharge delay, recharge area, local depressions filled with water, as well as soil moisture, contribute to deviations in time shifts and recovery times within the study area. The average recovery time of grassland is approximately 3.97 months (121 days), while for cropland it is 3.64 months (111 days). The drought timing is shown to be important in the recovery time. The later a drought ends in the growing season, the longer the vegetation regeneration time. Between the drought time or intensity and the vegetation regeneration time, no significant correlation was found, as soil moisture presumably dominates the drought recovery time. The results of this study provide insight into the vegetation recovery time of both grassland and cropland. Understanding these dynamics is crucial for enhancing large-scale hydrological models, such as PCR-GLOBWB 2.0, by incorporating accurate estimates of vegetation water demands during post-drought periods. As soil moisture is projected to decline further in the future, this research highlights the significance of acknowledging extended periods for drought recovery, thereby contributing to a more comprehensive assessment of the potential impacts of drought on vegetation regeneration for better sustainable water resource management.

Contents

1 Introduction

Droughts are an unpredictable natural phenomenon that affects many aspects of society and the environment globally. Due to ongoing climate change and anthropogenic drivers, extreme weather events, such as droughts and floods, have accelerated and intensified over the last decades. The number and duration of severe drought events are expected to increase even further in the 21st century (Wang et al., 2014). As a result, the percentage of the world exposed to severe drought events will increase from 5% to 40% (Burke et al., 2006). Severe drought can have devastating effects, such as significant crop yield losses, an increased risk of forest fires, exacerbated and intensified land degradation and desertification, and increased competition for resources.

The impact of droughts on crop production has become more pronounced over the last few years. A study by Wang et al. (2013) showed that Nepal suffered a severe winter drought in the years 2008 and 2009, which caused agricultural production to decline by 50%. In the year 2002–2003, India faced one of the worst and most exceptional drought episodes which made the land incapable of cultivation throughout the year. Whereas 68% (over 600 million) of the people are dependent upon agriculture in those regions and were therefore severely affected (Dutta et al., 2015). In Europe, the annual economic losses associated with drought are growing, reaching on average 6.2 billion euros per year during recent decades (Potopová et al., 2016). During the 2012 drought in the US nearly two-thirds of the country was affected by drought. Drought conditions were the most severe in the West, Great Plains, and Midwest where most of the agricultural production in the US occurs. In this year the agricultural losses were estimated at $30 billion (Rippey, 2015)

In various regions across the globe, food shortages are already occurring due to population growth. With the impact of droughts, it is expected this issue will be exacerbated. Population growth and economic development create more pressure on global water demands (Vörösmarty et al., 2000). In combination with climate change and changing precipitation amounts, water shortages will occur at more locations in the future which can lead to more frequent droughts (Trenberth, 2008). These droughts will have a major impact on agriculture which is the primary source of livelihood in many regions (Li et al., 2009; Lesk et al., 2016). To create sufficient crop production for population growth irrigation is used. Currently, it is the sector that consumes most of the renewable water resources (Tsur, 2005; Chirouze et al., 2014). With a better understanding of the magnitude and duration of droughts on vegetation growth, large-scale models such as PCR-GLOBWB 2.0 (Sutanudjaja et al., 2018) can be improved, and better estimations of potential water shortages can be made. Currently, PCR-GLOBWB 2.0 (Sutanudjaja et al., 2018) simulates irrigation with generalized equations to ensure crops receive the correct amount of water under typically climatic conditions. In the case of a drought, the crop dies, and water is no longer provided to these cells until the next rain event. This simplification is useful in calculating water demand; however, after a drought, vegetation needs time to recover and regrow resulting in a post-drought period with reduced water demand.

Keyantash and Dracup (2002) defined three types of droughts with slightly different criteria; meteorological drought which results from precipitation deficits, agricultural drought which is identified based on total soil moisture deficits, and hydrological drought which is related to a shortage of streamflow. All these types of droughts occur during a period of insufficient precipitation, but agricultural and hydrological droughts also include a shortage of soil moisture to replace losses by evapotranspiration which is critical for crop growth (Yao et al., 2023). Diverse vegetation types respond differently to drought. Generally, crops have a shallow root system which means it is dependent on the top part of the soil for water. Natural vegetation is most of

the time deeper rooted and therefore longer connected to the water table causing it to recover faster from a drought. Generally, insufficient precipitation causes water stress, in combination with high temperatures this affects plant health and heat stress (Chirouze et al., 2014). The recovery of vegetation to pre-drought conditions is largely dependent on the drought timing relative to the growing season. The growing season is important for the evapotranspiration and thus the soil moisture, which determines whether vegetation recovery occurs within a single or multiple growing seasons (Li et al., 2023).

Several indices that include different climatic variables, such as precipitation, temperature, and soil moisture have been developed to indicate droughts globally. The most widely used are the Palmer Drought Severity Index (PDSI), the Standardized Precipitation Index (SPI), and the Standardized Precipitation-Evapotranspiration Index (SPEI). The PDSI is developed by Palmer (1965) and incorporates antecedent and current precipitation, evapotranspiration, and a physical water balance model. However, a major limitation of the PDSI is that it calculates droughts on a fixed time scale of $\sim$ 12 months. This means it cannot accurately analyze meteorological and agricultural droughts that occur over shorter time scales. The SPI does not have this problem as it calculates droughts at different time scales only using the precipitation. Therefore, this drought index can be used for meteorological, agricultural, and hydrological applications. The SPEI is an advanced version of the SPI, based on a monthly climatic water balance (i.e., precipitation minus evapotranspiration) which means both precipitation and temperature variables are included for calculating droughts at different time scales. As a result, droughts can be monitored with respect to severity, duration, onset, extent, and expiration (Potop et al., 2012).

In the study of Joo et al. (2017), four plant species (switchgrass, miscanthus, prairie and maize/soybean) were monitored during the 2012 US drought. The initial response of the species was different, mainly due to their different rooting depths. However, as drought intensified, the evapotranspiration rates drastically declined which resulted in a large water deficit. During and after the drought, vegetation recovery and evapotranspiration lagged associated with the depleted soil moisture. Evapotranspiration rates vary with water availability and the physiological status of plants. During these post-drought periods, evapotranspiration rates will be low in the beginning and increase as vegetation recovers (Davis et al., 2017). Different factors such as drought severity, duration and soil moisture are of interest for the ecosystem stability (Schwalm et al., 2017).

With further global warming and the increase in drought events, it is important to understand not only the impact of droughts on vegetation but also the regeneration of vegetation in post-drought periods. With the increasing frequency of drought events, regions with longer vegetation recovery times are more likely to be exposed to new drought events before they are fully recovered. When ecosystems cannot fully recover they are more susceptible to experience a gradual loss of vegetation during future droughts and transition into a new equilibrium state (Xu et al., 2021; Huang et al., 2015). The combined effects of drought severity, duration and the length of drought recovery have the most impact on the ecosystem health and are responsible for their transitioning (Jiao et al., 2021; Fathi-Taperasht et al., 2022; Müller and Bahn, 2022; Yao et al., 2022).

Historically, no research has been done on crop regeneration and there is limited research on vegetation regeneration after a drought (Anderegg et al., 2015; Schwalm et al., 2017; Yu et al., 2017; He et al., 2018; Liu et al., 2019; Yao et al., 2022, 2023). With the increasing pressure on water demand and food security, the regeneration of crops can be vital in estimating crop yields, subsequent food security, economic output, and water availability globally.

Therefore, the current study aims to analyze vegetation regeneration after droughts with the

help of a drought and vegetation index. An additional objective of the study was to determine whether soil moisture impacts vegetation regeneration in the post-drought periods.

2 Methods

2.1 Study area

The research focuses on Nebraska, a state in the United States with the highest agricultural receipts and the most irrigated land (14.8 percent of all irrigated cropland in the United States (USDA, 2022)). It is part of the Great Plains, the region that was severely hit by the 2012 drought (Lal et al., 2012). This drought was caused by the back-to-back La Niña episodes of 2010–11 and 2011–12. The U.S. corn yield was reduced by over 25 percent during this event (Rippey, 2015). Due to this intense drought, a large range of crop recovery times is expected.

Figure 1 shows the land cover of the study area in 2020. The east of Nebraska predominantly consists of croplands (95 to 98 °W), primarily featuring cropland rainfed herbaceous cover. Towards the west (98 to 104 °W), the land cover almost entirely consists of grassland. This is the region where the Great Plains start and the elevation increases. At 41 °N, the North Platte River runs from west to east through the study area. Around this river large cropland areas are present. This is due to the large amount of irrigation wells present in the basin (NeDNR, 2023), which are mainly placed along the river because of the good accessibility and water quality.

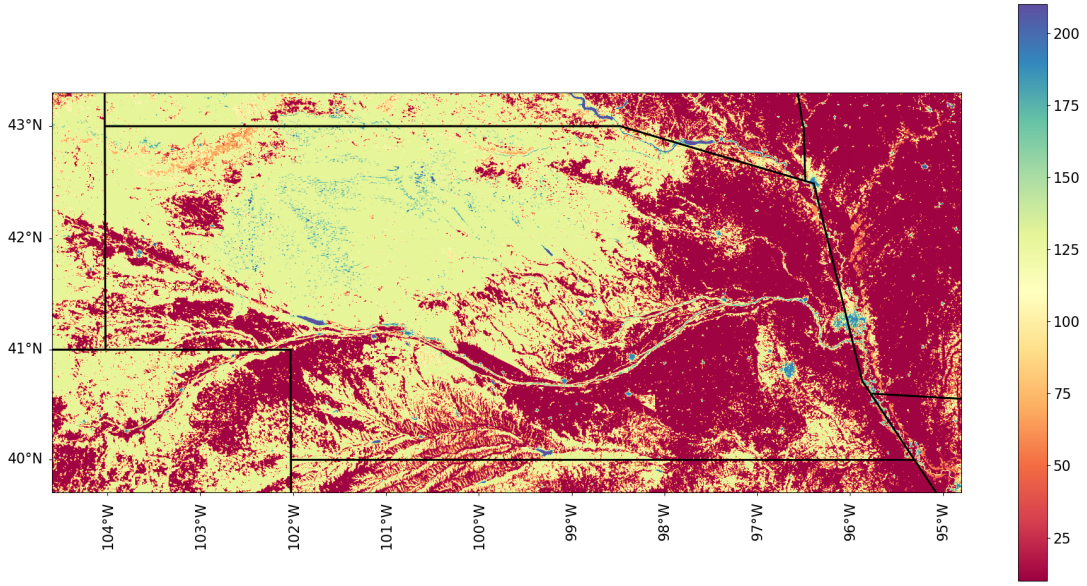

Figure 1: Land cover of Nebraska (Copernicus Climate Change Service, 2019). Land cover classes in Appendix table 1

2.2 Datasets

Datasets used in this study are carefully selected based on their characteristics and resolution. For land cover classification, global datasets such as Modis, ESRI LULC (ESA), Global Land Cover Network (GLC-SHARE) and also the national dataset MRLC (NLCD) were considered. Even though some had the advantage of a smaller resolution size, the classification was not as comprehensive as in the ESA CCI LC dataset. Here a separation between irrigated and rainfed cropland was made, which is considered quite important in this study, therefore the ESA CCI LC dataset is used in the research.

For drought indices, a broad spectrum of datasets has been developed over the years. The most common ones are the SPI, SPEI, PDSI and the Palmer Z-index. Both the PDSI and the

Palmer Z-index have a timescale between 9 and 12 months, while SPI and SPEI are available for timescales between 1 and 48 months. As vegetation recovery is expected to occur in a few months after a drought, shorter timescales are expected to be of greater relevance in this analysis. The SPEI dataset is selected over the SPI due to its enhanced features (section 2.2.2).

The vegetation canopy greenness is available in NDVI, kNDVI and EVI datasets. EVI is the only dataset with corrections for some atmospheric conditions and canopy background noise. But is also more sensitive in areas with dense vegetation. Therefore, this is the most suitable dataset to use in the research.

At a global scale, multiple soil moisture datasets are available from different satellites, e.g. AMSR2, ASCAT, Sentinel-1, SMAP, SMOS, ESA-CCI, and LSM. These products differ in terms of spatiotemporal resolution, coverage, and data sources. The ESA-CCI dataset has the largest temporal availability and is therefore used for the analysis.

All datasets were accessed on 10-07-2023 (July 10, 2023). Due to different temporal availability, there is chosen to analyze all the data from 2003 to 2020.

2.2.1 Land cover dataset

The global land cover (LC) dataset is released by the European Space Agency (ESA) Climate Change Initiative (CCI) (Copernicus Climate Change Service, 2019). The ESA CCI land cover dataset contains 29 consistent global land cover maps on an annual basis from 1992 to 2020, with a spatial resolution of 300 m. This small spatial resolution and extensive classification on a global scale have made it attractive to use in this study. The land cover dataset is divided into 22 classes which have been defined using the United Nations Food and Agriculture Organization's (UN FAO) Land Cover Classification System (LCCS). The complete legend with land cover classes is given in Appendix table 1.

2.2.2 SPEI dataset

SPEI (Standardized Precipitation Evaporation Index) is an index representing the degree of drought obtained by quantifying precipitation, potential evapotranspiration, and temperature. A positive SPEI indicates wet conditions, and a negative SPEI indicates dry conditions. Most studies related to drought analysis have used either the Palmer Drought Severity Index (PDSI) (Palmer, 1965) or the Standardised Precipitation Index (SPI) (McKee et al., 1993). SPEI is a relatively new drought index formulated based on precipitation and PET (Potential evapotranspiration) (Vicente-Serrano et al., 2010). The SPEI is similar to the standardized precipitation index (SPI), but it includes the role of temperature. This means an increase in water demand as a result of increasing evapotranspiration rates can be identified by this drought index and correspond to higher drought intensities. The temporal resolution of this dataset is monthly and the spatial resolution is 0.5°, data is available from January 1901 to June 2023. SPEI is available on multiple timescales (1, 3, 6, 12 and 24 months), in this research the 3-month SPEI is used. The 3-month SPEI is based on the cumulative water deficit or surplus over the preceding 3 months. For this research, it is expected that the hydrological droughts, in combination with soil moisture conditions which respond to precipitation variances on a relatively short timescale, show the best signatures. Therefore, the 3-month timescale was chosen for the SPEI data.

2.2.3 EVI dataset

The Enhanced Vegetation Index (EVI) (Didan, 2015) shows the vegetation canopy greenness, which is a composite property of canopy structure, chlorophyll and leaf area. EVI is developed as an improvement upon the Normalized Difference Vegetation Index (NDVI), it corrects for some

atmospheric conditions, takes changes in canopy structure into account and is more sensitive in areas with dense vegetation. These improvements provide a more accurate and comprehensive measure of vegetation health and vigor. EVI data is produced on 16-day intervals and with a spatial resolution of 5.6km. Preprocessed data was available from 2003 to 2021.

2.2.4 Soil moisture dataset

The ESA-CCI soil moisture (SM) (Dorigo et al., 2023) data was developed to provide a long-term climate data set for evaluating long-term trends. Hydrological and agricultural processes, runoff generation and drought development are all influenced by soil moisture. In this study, soil moisture was used to evaluate vegetation sensitivity to soil moisture in post-drought periods. Hereby, the ACTIVE product, version 08.1 was used, which covers a period from 05-08-1991 to 31-12-2022. The product is representative of the first few centimeters of soil ($\sim 0 - 5$cm) and is provided in percent of saturation [%], with a spatial resolution of 0.5°. From the daily soil moisture data, a monthly average was calculated, this had to do with the processing time of all daily files.

2.3 Smoothing of data

There is noise present in the time series of SPEI, EVI and SM, to reduce this a smoothing window was used. In this case, it was decided to use the Hanning window. This is a weighted average window that is mostly used in signal processing and data analysis. The Hanning window allocates greater weight to central data points while gradually reducing influence towards the window boundaries. By using this smoothing there is a refined balance between noise reduction and the retention of essential signal features. In this research, the length of the Hanning window was set at 6 months, due to different temporal resolutions the actual window length differs between the datasets. For example, the length of the smoothing window for SPEI and SM is 6 because the temporal resolution is monthly. While for EVI the length of the smoothing window is 12, due to the temporal resolution of 16 days.

In the time series of the soil moisture gaps occur, depending on the location. These gaps can occur when there are no meaningful soil moisture retrievals, for example in areas with dense vegetation, large fractional coverage of water or ice, strong topography, or extreme desert areas. When there are no values available the smoothing window brings the time series of the soil moisture gradually to 0%. These values, although not representative of reality, are unavoidable in the presence of data gaps. In the study area used in this research, there is no data available during the winter months (e.g. December, January and February), this is most likely due to snow coverage.

2.4 The identification of drought events and recovery time

To identify drought events and vegetation recovery the SPEI and EVI were used. To sort all the data into different vegetation types the LC was used. To prevent any generalization in the LC data, the datasets of SPEI, EVI and SM were converted to a 300m spatial resolution. The corresponding data analysis was done pixel by pixel in Python.

First, drought events were identified, droughts were considered to begin when SPEI was less than -0.5 and end when SPEI was greater than -0.5. Because the SPEI data was monthly available, an interpolation was performed when the SPEI intersected with the threshold of -0.5. On top of that, three conditions were set to prevent incorrect data from being used in the

analysis. I) When there is less than 1 month between two droughts, they are combined into one drought. Ecosystems cannot recover on such short notice, so in most cases, the first drought already has a significant impact (Yao et al., 2022). Therefore, they are combined and considered as one drought. II) Drought events have to last at least 1 month. The temporal resolution of SPEI is monthly, a drought time of less than 1 month would result in only one data point falling below the threshold. This leads to inaccurate estimations of drought time, and the drought event would not last long enough to make a serious impact on the vegetation greenness. III) The drought has to start and end within the time series. If the time series starts with SPEI below -0.5 or/and ends below -0.5, the drought is removed. The drought time and intensity can not be accurately calculated from these drought events and would therefore distort the data of complete drought events.
Once the droughts were determined, the drought intensity was derived from the SPEI data. The drought intensity is the minimum value the SPEI reaches during a drought event. This is done to determine whether not only drought time but also drought intensity correlates with vegetation recovery time.

Secondly, the corresponding vegetation anomalies in the EVI data are identified. With the help of the *statsmodels.tsa.seasonal.seasonal_decompose* package in Python, the seasonality is removed from the EVI data. Hereby the additive model is used, this means the magnitude of seasonality does not change over time. By entering the period, which should correspond to an entire seasonal cycle, the package identifies the trend of the seasonal cycles over the entire time series. In this case, the EVI data has an annual resolution of 23, and therefore the period is set to 23. The package also filters out the residual noise, to only remain with the trend of the time series. From this trend, the mean and standard deviation (SD) are calculated. Then the SD is subtracted from the mean, to visualize negative vegetation anomalies. With this new threshold (-SD), regular declines in vegetation caused by grazing or harvesting are not counted as negative vegetation anomalies. Also in this time series, the negative vegetation anomaly was removed when the start of EVI was below the -SD or/and ended below the -SD. To prevent incomplete vegetation recovery times from being used in the data analysis.

Thirdly, a coupling between identified droughts and negative vegetation anomalies was made. The samples with droughts but no negative vegetation anomaly within six months after or one month before the drought started were removed. Just like samples with negative vegetation anomalies but no droughts within six months before or one month after the start of the negative vegetation anomalies were removed. Only samples with drought and a negative vegetation anomaly within six months after or one month before the start of both, are selected for the analysis. Figure 2 shows two events where a drought and negative vegetation anomaly match. These are the 2006 and 2012/2013 drought, the other grey-colored areas in figure 2 have no matching events and are therefore not included in the analysis. When there a multiple negative vegetation anomalies within this boundary, the duration of every single anomaly is calculated and the longest one is selected for the corresponding drought. In the few cases where multiple droughts correspond to one negative vegetation anomaly within this boundary, the process was converted and the longest drought was selected.

Lastly, the vegetation regeneration time was calculated, this was done in two different ways. Within a negative vegetation anomaly, the minimum value and the corresponding date are determined. The vegetation recovery time starts from this 'minimum' date and ends when the EVI time series is greater than the -SD. This will be called the 'first method' and is shown with the purple arrow in the highlighted section of figure 2. In the 'second method' the end of the recovery time remains the same. Only the start is determined differently, the end of a drought is classified as the beginning of the vegetation recovery period. This method is shown with the dark green arrow in the highlighted section of figure 2.

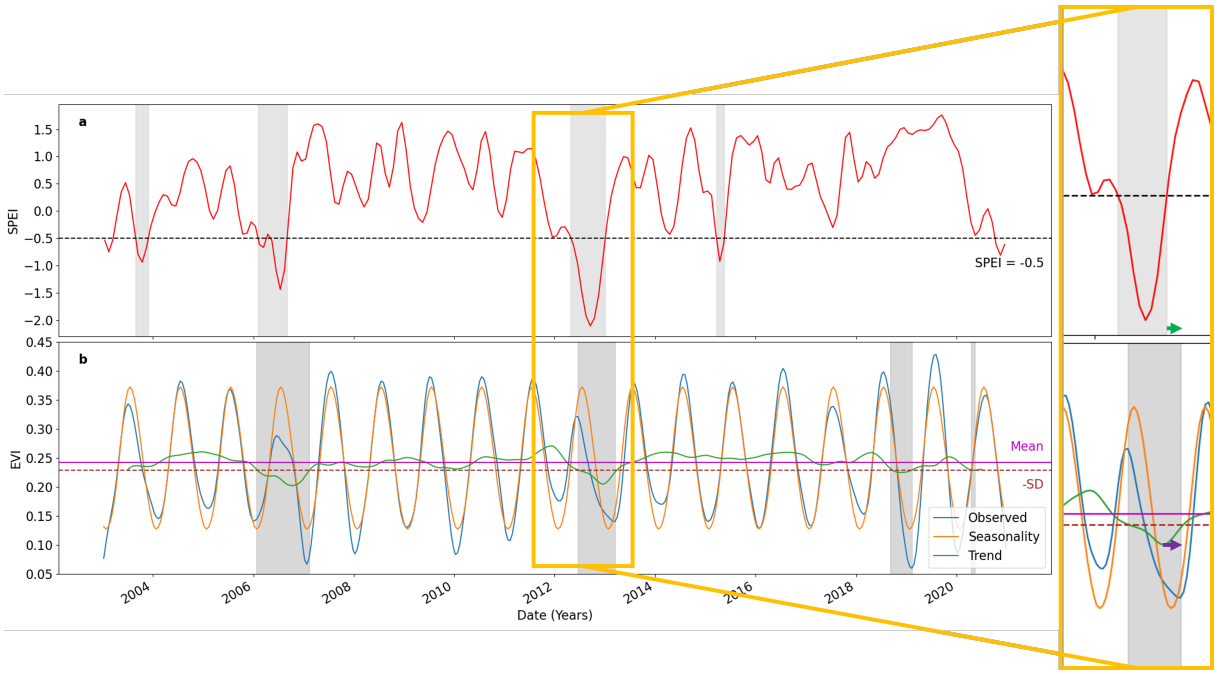

Figure 2: a) SPEI time series, droughts indicated in grey. b) EVI time series, negative vegetation anomaly indicated in grey. The highlighted section provides a magnified view, with two arrows indicating the methods used for the calculation of vegetation regeneration time

2.5 Cross-correlation

To analyze how well the SPEI and EVI data match a cross-correlation is carried out. This is done with the *numpy.correlate* function. The inputs for this function are the SPEI data and the deseasonalized EVI data. Because the SPEI data has a different temporal resolution and is measured at different dates compared to the EVI, it first had to be interpolated to the same dates. For this interpolation, the unsmoothed SPEI time series is used. This gave some slight, but no significant, changes in the time series. To correctly smooth the data for this correlation, the Hanning window length was set to 12 for both the SPEI and EVI time series.

Before the two time series were cross-correlated, they first had to be standardized. By standardizing these time series all values range between -1 and 1. For this the commonly used standardization is used:

$$\mathrm{EVI}_{\mathrm{standardized}} = \frac{\mathrm{EVI} - \mathrm{Mean}}{\mathrm{SD} \times \mathrm{length(EVI)}}$$

$$\mathrm{SPEI}_{\mathrm{standardized}} = \frac{\mathrm{SPEI} - \mathrm{Mean}}{\mathrm{SD}}$$

Between these two standardized time series the cross-correlation was made. From this correlation the maximum value was extracted, which represents the best possible fit between the time series. The time between the best possible fit and the original time series is referred to as 'time shift'. So, this represents the number of days to shift the SPEI over the EVI time series to the best possible fit. Because this applies to the entire time series, it may give a distorted picture for droughts. Therefore, a correlation is also made for parts of the time series where droughts were present. The start of this selection is the beginning of the drought (SPEI below -0.5) and ends when the negative vegetation anomaly ends (above -SD).

3 Results

3.1 Dynamics of time series grassland and cropland

Figure 3 shows the time series of the drought index and the vegetation greenness for grassland. During wet periods the EVI goes above the mean and during dry periods it goes below the mean and even below the -SD threshold when the drought is severe, this shows the EVI is responsive to the SPEI. The extreme 2012/2013 drought is visible in the SPEI and also causes an immediate response from the EVI, in which the vegetation greenness goes far below the mean. The 2006 drought causes the EVI to decrease but not below the threshold, after a short wet period the SPEI decreases to approximately 0. This wet period was not long enough for the vegetation to recover from the drought, as the EVI went below the threshold in 2007. These vegetation responses are not included in the analysis as the SPEI does not fall below the threshold but it shows the frequency of drought periods also has an impact on vegetation greenness. The short droughts in figure 3 also create a response in the EVI but only to deviate around the mean, so from this time series only the 2012 drought is used in the analysis.

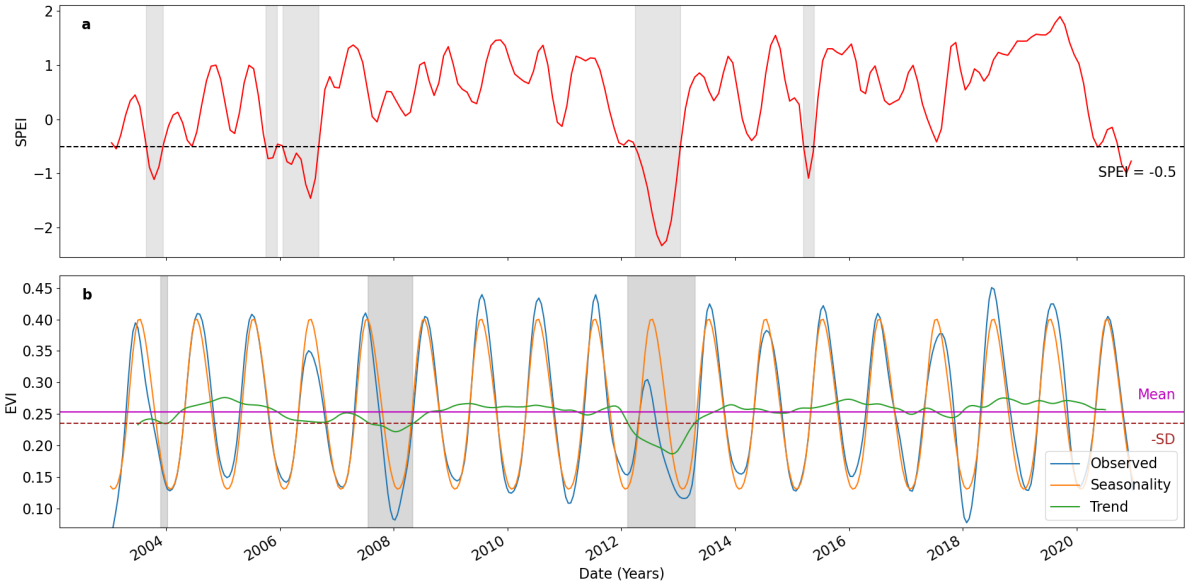

Figure 3: Time series of SPEI and EVI for grassland at location 40°48'00.0"N 100°27'00.0"W

Figure 4 shows the time series of the drought index and the vegetation greenness for cropland. For cropland, the EVI also responds to the SPEI, but patterns that cannot be explained by droughts also arise. The small droughts at the beginning of the time series are not visible at all in the EVI, most likely due to irrigation. The 2012 drought also appears in this time series such as the 2006 drought and the aftermath in 2007, which caused the vegetation greenness to remain below the -SD threshold for a considerable duration. During the winter of 2008/2009, the EVI was higher than average, while in the winter of 2009/2010 it was suddenly far below the mean. This trend is absent in the SPEI as no prolonged wet or dry periods occur at this time. In the study of Fontana et al. (2007) a similar occurrence was observed and linked to the cultivation of winter crops. The winter crop area fluctuates from one year to another and is therefore not consistent over the time series. For this area, winter crops were likely cultivated in 2008/2009, resulting in a high vegetation greenness. Conversely, in 2009/2010, the area was presumably left bare, resulting in a low vegetation greenness. These vegetation responses in cropland are not included in the analysis as the SPEI does not fall below the threshold but it shows that anthropogenic influences change the vegetation greenness in the area. As a result,

vegetation recovery times may not be uniform across the time series.

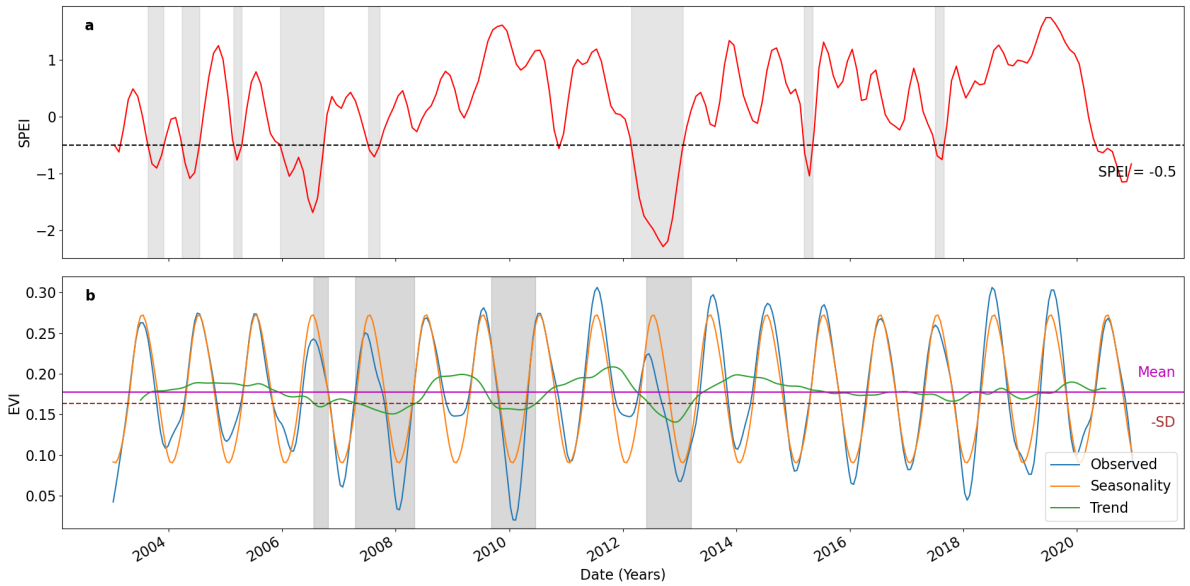

Figure 4: Time series of SPEI and EVI for cropland at location 40°36'00.0"N 102°00'00.0"W

3.2 Drought impact on vegetation greenness

The land cover pattern is reflected in the relation between the drought index and the vegetation greenness, as expected from the time series in section 3.1. The correlation values for the best fit are shown in figure 5a. The correlation coefficient is below 0.4 for all unnatural vegetation types, i.e. cropland. In natural vegetation, a striking difference is present. Grassland shows correlation values higher than 0.5. Especially in the middle of Nebraska, between 41 to 42 °N and 98 to 102 °W, the correlation coefficient is high as it approximately reaches 1.0. Towards the northwest where the elevation increases, the correlation becomes lower. Still, the correlation coefficient in the entire study area is higher for grassland than cropland. In the northwest corner of Nebraska, a relatively small area is covered in natural vegetation consisting of trees or other tall vegetation. This area shows the same poor correlation as the cropland. In figure 5b this area, such as most of the cropland is grey. Meaning that there was a negative time shift. These areas are masked, because it does not make sense if negative vegetation anomalies occurred before droughts. The cropland areas that are not masked show a contrasting image. They have a time shift of larger than 200 days for the best correlation coefficient. These values do not correspond at all to the natural grassland that surrounds these areas.

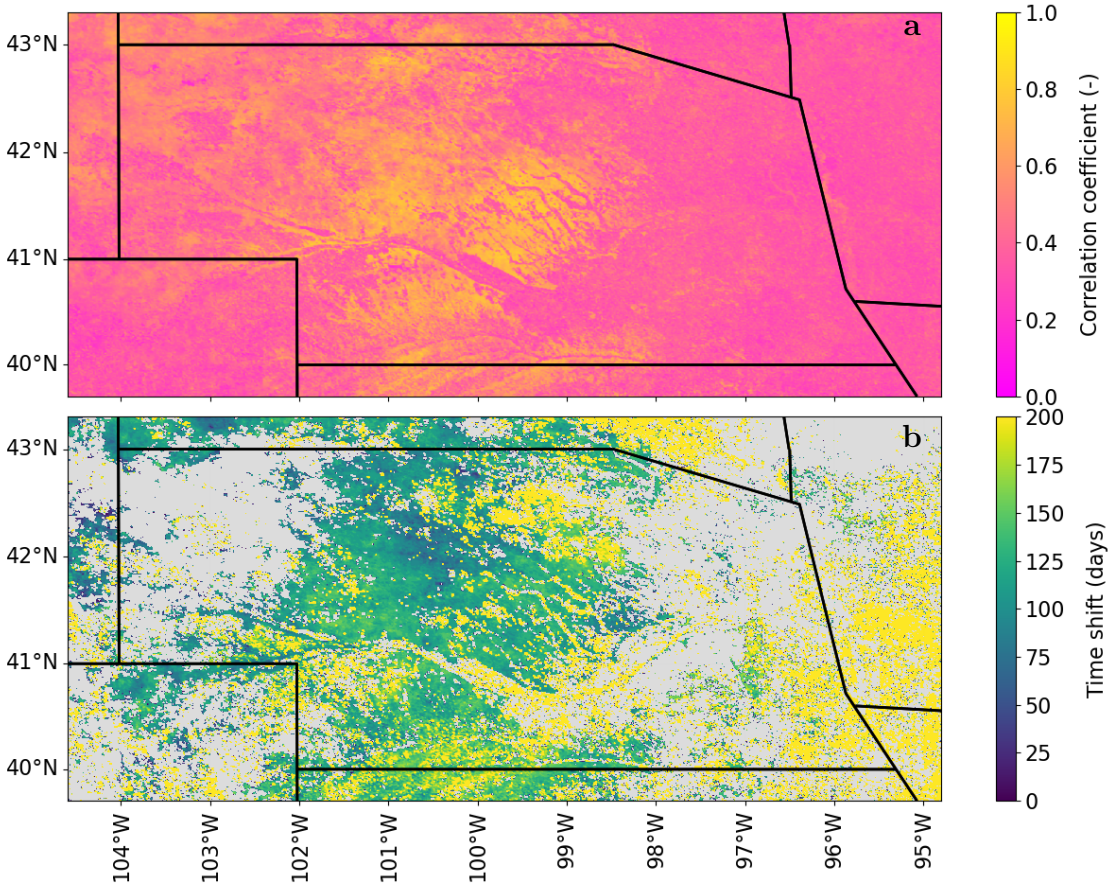

Figure 5: Cross-correlation between drought index and vegetation greenness. a) Highest possible Correlation coefficient (-) for the cross-correlation. b) Time shift (days) between the two datasets at the highest possible correlation coefficient

For the areas with a low correlation coefficient, it is difficult to accurately estimate the time shift. All areas where the correlation coefficient is lower than 0.4 have a time shift that is negative or higher than 200 days. In the center of Nebraska where the Great Plains start (41 to 42 °N, 98 to 102 °W) the time shift shows more accurate values. Around the North Platte River, it is on average 125 days, further north the time shift decreases to an average of 75 days.

This same cross-correlation is also carried out for selected time periods. Namely, from the beginning of the droughts till the end of the vegetation recovery (end of negative vegetation anomaly). The results of this correlation are shown in figure 6. The white areas mean there was no drought corresponding to a negative vegetation anomaly. Most of these no data points are in areas with cropland. For the cropland areas where the correlation coefficient is calculated, the values are again lower than for natural grassland. The correlation coefficient for cropland is on average 0.5, for grassland it is around 0.8 and in some areas even up to 1.0. In figure 6a the correlation coefficient for grassland in the center of Nebraska is around 0.8, but is increasing towards the northwest. While in figure 5a the values are decreasing in that direction.

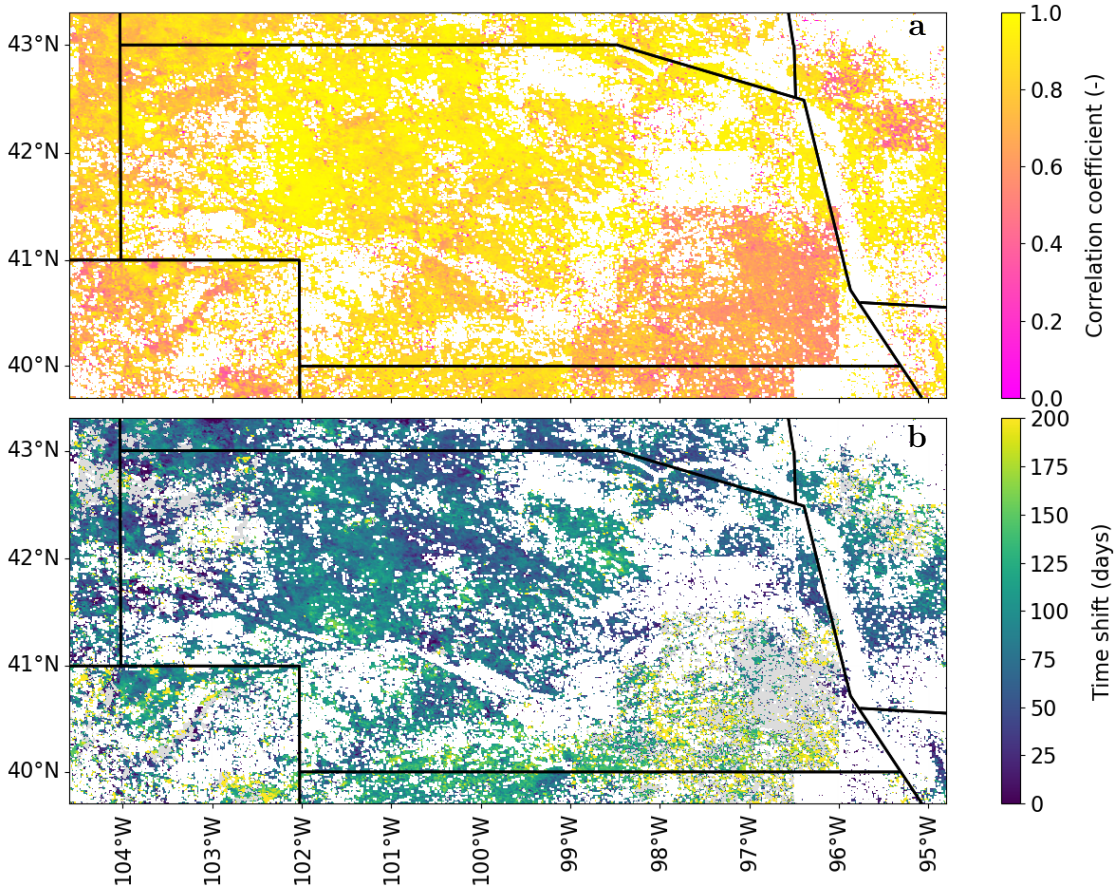

Figure 6: Cross-correlation between droughts and negative vegetation anomalies. a) Highest possible correlation coefficient (-) for the cross-correlation. b) Time shift (days) between the two datasets at the highest possible correlation coefficient

The time shift for cropland areas in this correlation also differs from the rest. Again almost all values for the time shift are negative or larger than 200. These time shifts match the lower correlation values of figure 6a. North of the North Platte River, again the slight decrease in time shift is visible but it is less pronounced than in figure 5b. The regions covered by grassland with a higher correlation coefficient generally show a larger time shift, on average between 100 and 125 days. For the regions with a slightly lower correlation coefficient, the time shift is also smaller, on average varying between 25 and 100 days.

The angled pattern in figure 6 is due to the satellite resolution. This is visible in the southeast corner of Nebraska, where the cropland shows low correlation values and time shifts that differ compared to the surroundings. Because the SPEI dataset has the largest spatial resolution it will dominate the angled pattern in the figure.

3.3 Impact of drought length and intensity on vegetation regeneration time

The predominant vegetation types in the study area are grassland and cropland rainfed herbaceous cover. These two vegetation types are therefore used to analyze the impact of drought length and intensity on vegetation recovery. The error bars in figures 7 and 8 represent a 90 percent confidence interval (5th percentile to 95th percentile). Values can deviate far around the mean but the extreme outliers, which are potentially incorrect but not filtered out by this method, are not displayed by this confidence interval.

Figure 7a, b and c show the vegetation regeneration time of grassland based on the drought

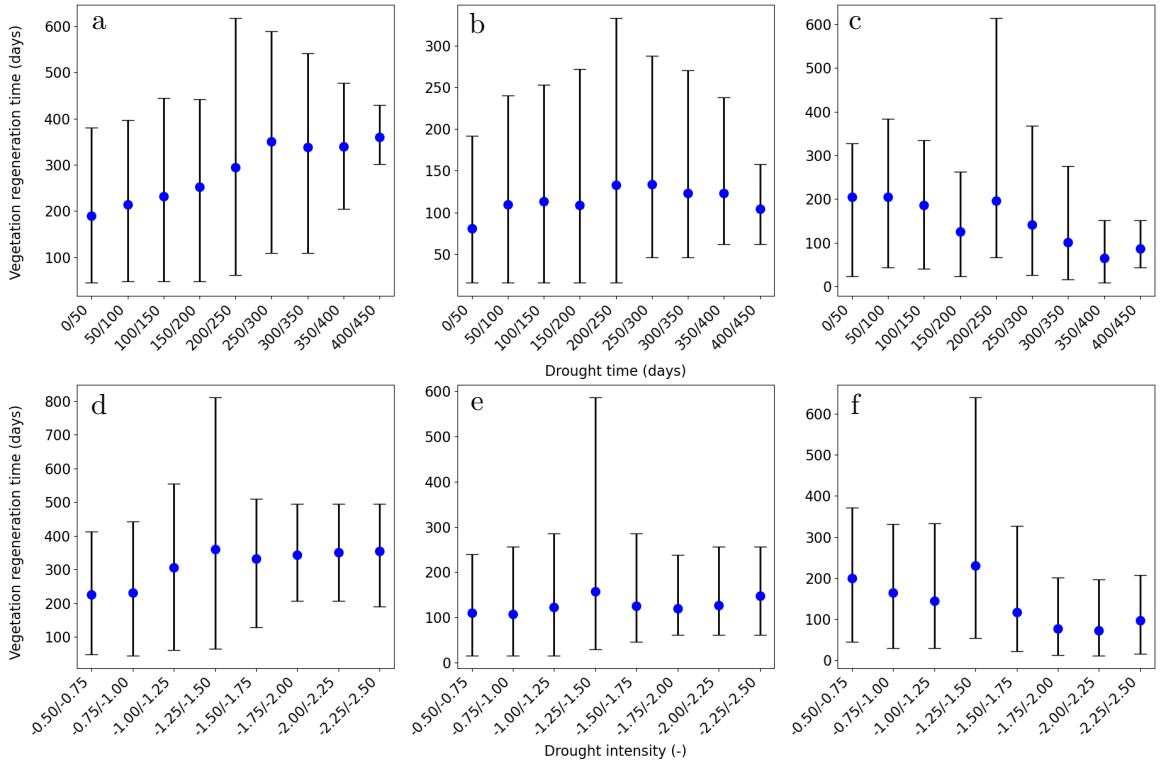

Figure 7: Vegetation recovery of grassland classified by drought length and intensity. a-c) Recovery time based on drought time. d-f) Recovery time based on drought intensity

time. While figure 7d, e and f show the vegetation regeneration time based on drought intensity. The vegetation regeneration time of figures 7a and d is the time of the negative vegetation anomaly. the duration from the point at which the EVI falls below the -SD threshold until it surpasses the -SD threshold again. The vegetation regeneration in figure a increases from 190 to 350 days, for a drought time between 0 and 300 days. Despite the increasing drought time from this point up to 450 days, the vegetation recovery remains relatively consistent around 350 days. Figure d shows a similar pattern, the vegetation recovery time increases for a drought intensity between -0.5 to -1.5, but then the recovery time also stabilizes around 350 days for higher drought intensities. Figures 7b and e show the vegetation recovery time calculated with the 'first method', mentioned in section 2.4. The minimum value in the negative vegetation anomaly and the corresponding date are determined. The vegetation recovery time starts from this 'minimum' date and ends when the EVI time series is greater than the -SD. Using this method, there is no clear relation visible between the drought time or intensity and vegetation regeneration time. The recovery time remains around the mean of 121 days for all drought time lengths and intensities. In figure b the error bars increase in range till the 250 days of drought time, and then they become smaller again. This is most likely due to the amount of samples available for the analysis. Most droughts have a length between 0 and 250 days, longer droughts are less common and will therefore have fewer outliers in the data. For the droughts in the category 400/450 days, the number of data points has become so scarce that the error bars show relatively accurate estimation for the vegetation recovery. Figures 7c and f show the 'second method', mentioned in section 2.4, to calculate the vegetation recovery time. The end of the recovery time remains the same but the start of the vegetation recovery period is set as the end of a drought. The limitation of this method was that the vegetation sometimes recovered before the drought ended. This produced negative values that distorted the analysis. To prevent this, the negative values were removed from the data. The vegetation recovery shows a remarkable

pattern, the vegetation regeneration time becomes shorter as the drought time or intensity increases. However, the mean recovery is slightly higher with this method, namely 135 days.

Figure 8 shows similar plots as figure 7, but these represent the vegetation recovery time of croplands. All these plots have a capricious pattern in comparison to figure 7. The vegetation regeneration time of cropland, calculated by the same two methods, generally shows the same trend as the one for grassland. In the figures 8b and e the values remain around the mean of 111 days for all drought lengths and intensities. In figures 8c and f the vegetation regeneration time declines as droughts elongate or become more intense. The mean recovery calculated by this method is 158 days. Only figures 8a and d do not show a similar kind of pattern. The vegetation regeneration time in figure a is quite high ($\sim$ 290 days) for drought times of 50/100 and 100/150 days. But shows a general increase during droughts from 150 to 450 days.

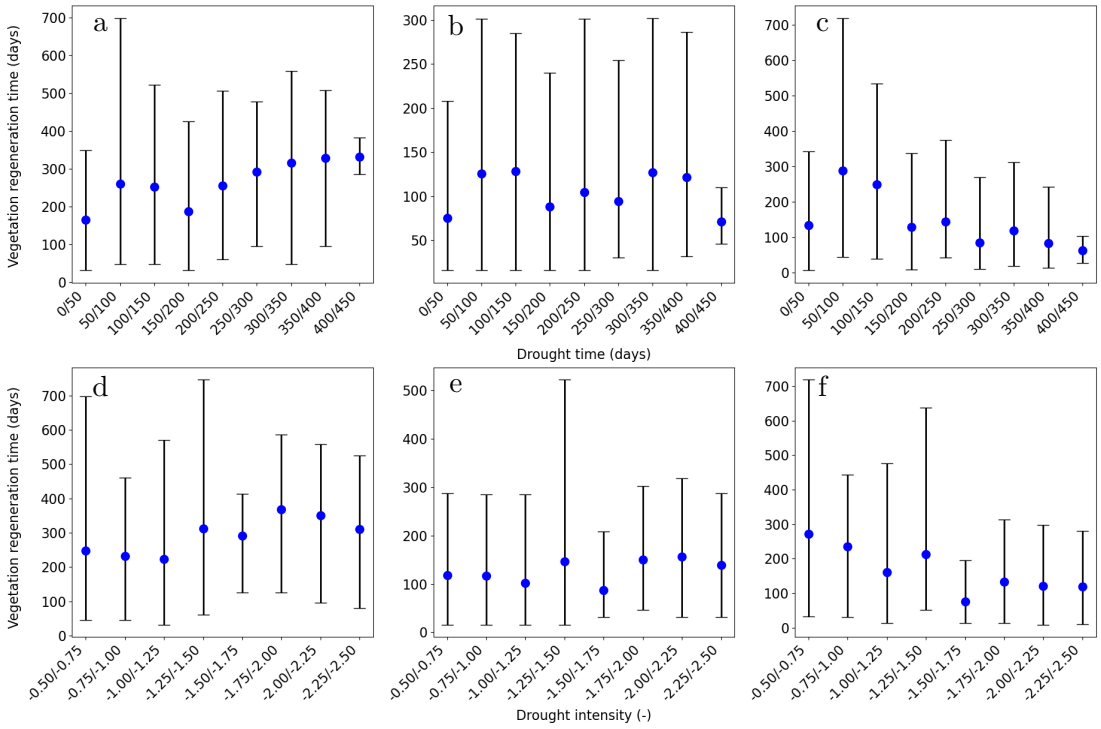

Figure 8: Vegetation recovery of cropland classified by drought length and intensity. a-c) Recovery time based on drought time. d-f) Recovery time based on drought intensity

3.4 Effect of drought timing on vegetation regeneration time

In addition to the drought length and intensity, the drought timing is also used to investigate the impact on the vegetation recovery time (Figure 9). For this analysis, the data calculated by the 'second method' (section 2.4) for vegetation regeneration time is used. The drought timing indicates the month in which the drought ended. Therefore, the 'second method' (section 2.4) was the most logical option as the vegetation regeneration time was already calculated from the end of the drought. For example, when a drought ends in January for the land cover type grassland, the vegetation has a mean recovery time of 78 days. This is just over 2.5 months, so the vegetation will be recovered between mid-March and mid-April (depending on when the drought in January ended). This mean recovery time was calculated for all months where the droughts ended.

The recovery time in both grassland and cropland show exceptionally high values for the months March and May, in comparison to the surrounding months. When these months are

excluded from consideration, both the graphs for grassland and cropland show a trend in vegetation regeneration time. For grassland, the vegetation regeneration time increases from 78 to 234 days, between the months January and October. In November and December, the recovery time declines fast towards 100 days. For the months September and October where the mean regeneration time is relatively high, also the error bars have a wide range. Especially towards the upper limit the regeneration time is uncertain. So, when a drought ends in these months recovery could take much longer than the average shows. Rainfed cropland shows a different pattern in the vegetation regeneration time (figure 9b). Here the regeneration time increases between February and July, from 85 to 296 days. Then it gradually decreases until December to 73 days. The months June to September show the highest regeneration time of around 275 days. The error bar of these months also indicates a wide range of values, meaning that the regeneration time is quite insecure.

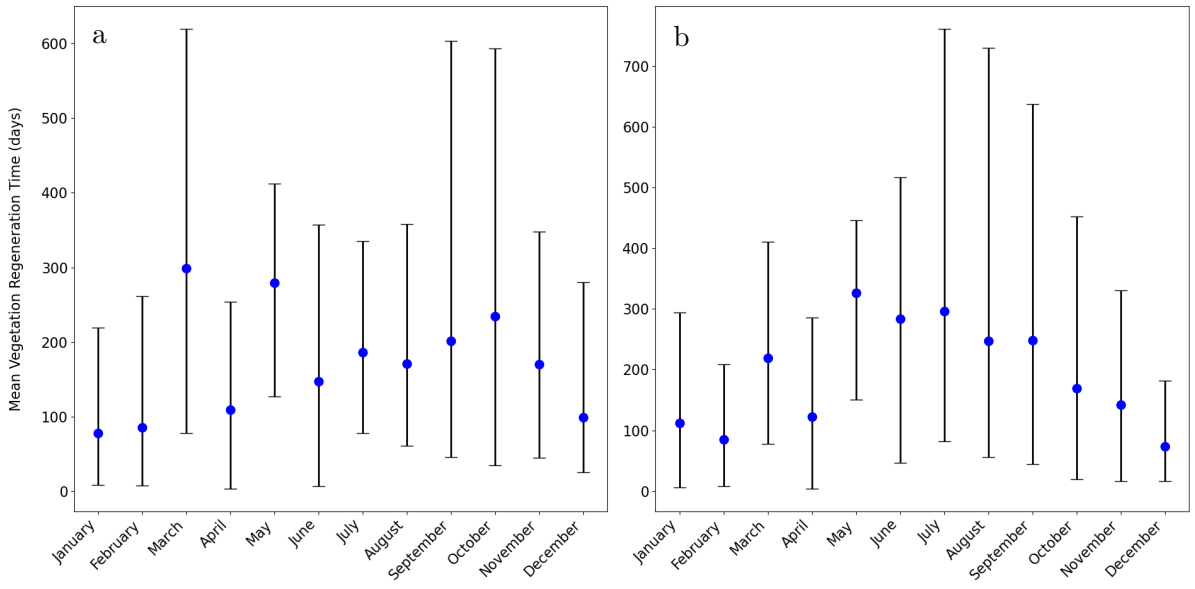

Figure 9: Vegetation recovery classified by drought timing. a) Grassland. b) Cropland

4 Discussion

4.1 Drought impact on land cover

The study area consists, after the conversion to the 300 m x 300 m spatial resolution grid, of 4,570,992 pixels per time step. During the 18 years in which the data analysis was carried out, a total of 36,290 pixels occurred with a change in land cover type. This means only 0.79% of the land cover has changed over all these years. The predominant transformation observed was the conversion of grassland (57%) to cropland rainfed herbaceous cover (41%). The majority of these transitions are most likely anthropogenic, as they evolved into rainfed cropland. Since it covers such a small area, the low correlation coefficients found in figure 6 are not caused by land cover changes.

The predominant land cover at lower elevations in the east of the study area is cropland rainfed herbaceous cover (figure 1). All areas classified as this land cover have correlation values lower than 0.4 (figure 5). However, higher correlations were expected for this land cover type, as rainfed crops depend on the amount of precipitation and are therefore impacted by droughts. In the study of Ray et al. (2018) results indicate that droughts had a more pronounced impact on the yield of rainfed crops compared to their corresponding irrigated crops. Not only the yield, but the whole physiology, growth and biomass production of crops is impacted by droughts. After 40 days the Leaf Area Index of rainfed crops starts to differ from irrigated crops. After 60 days, a significant difference between the crop types is visible (Delfine et al., 2001). Since the leaf area is a significant component in determining the vegetation greenness of the EVI, this difference should be noted after processing the data from the satellite sensors.

Taking a closer look at the land cover in figure 1 shows that no single pixel in the area is classified as irrigated cropland. According to USDA (2022), Nebraska has the most irrigated cropland in the United States. Because of this contradiction, a closer look was taken at satellite images of the area. The satellite image in figure 10 clearly visualizes that the area is covered with irrigated cropland. In the entire study area, many more regions like these are classified as rainfed cropland instead of irrigated cropland. This incorrect classification most likely explains the low correlation coefficient, as irrigated croplands have a minor drought response (Lu et al., 2020; Deb et al., 2022).

Due to this incorrect classification, the vegetation regeneration time for cropland in the figures 8 and 9 will not be completely accurate. Irrigated and rainfed cropland have a different drought response but are classified in the same class. This also explains the deviation of figure 8a and d, compared to figure 7a and d. The duration of the negative vegetation anomaly of cropland does not appear to be dependent on the drought time or intensity, unlike grassland. For irrigated cropland, this is a logical response but not for rainfed cropland, as it depends on climatic variables. No further separation could be made in the data analysis, as they were classified together in the land cover data. Different land cover classification datasets, such as Modis, ESRI LULC, MRLC or Global Land Cover Network were considered to be used in the research. However, due to a lower temporal or spatial resolution and also fewer land cover classes they were not suitable. On top of that, all these datasets made no distinctions between crop types. The ESA CCI land cover dataset was the only one to separate rainfed and irrigated cropland, but as shown in figure 10 there are quite large classification errors in this separation.

An accurate separation between these classes is important to evaluate the impact of droughts, mainly on rainfed croplands. The number and duration of severe drought events are expected to increase in the future (Wang et al., 2014). This leads to more water shortages, especially for rainfed vegetation. But the water demand of irrigated croplands will also increase (Zhang and Lin, 2016), which brings higher economical costs (Lopez-Nicolas et al., 2017). The increasing water demand will probably be resolved by extracting more groundwater. This mitigation

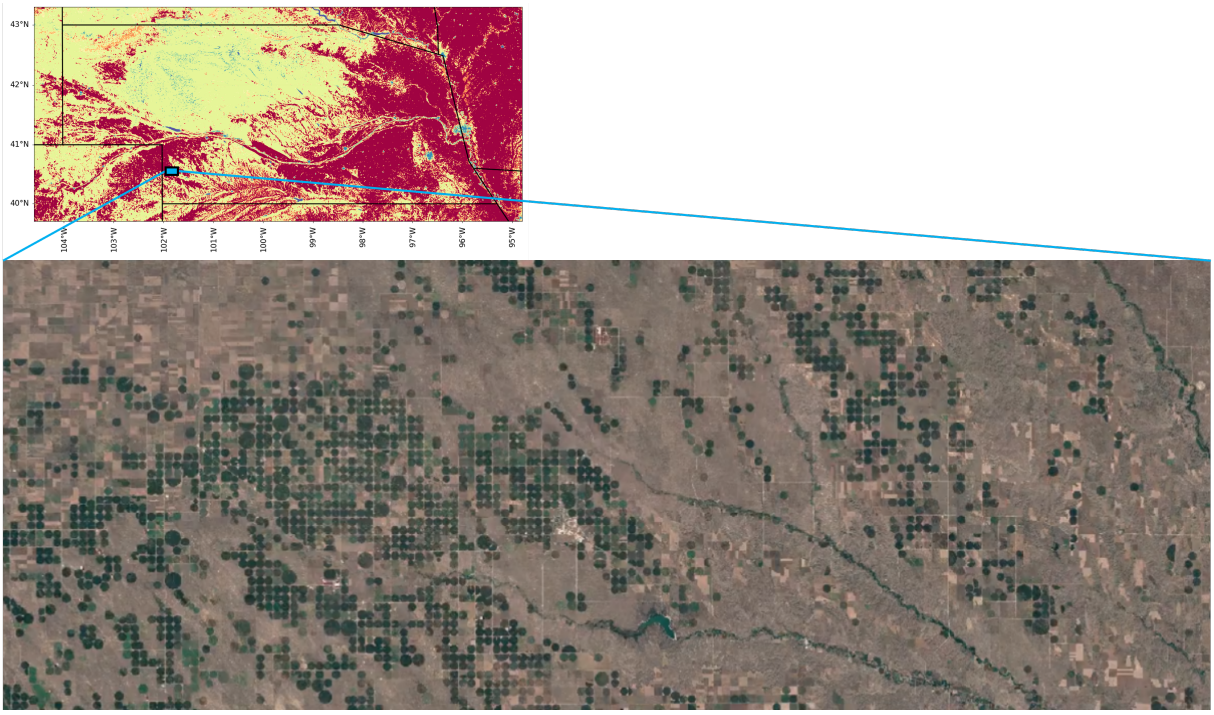

Figure 10: Satellite image of cropland in Nebraska (40°30'37"N 101°47'14"W)

strategy has major implications on nearby natural vegetated areas (Elmore et al., 2006). As groundwater levels decrease and aquifers are depleted (Konikow and Kendy, 2005).

The accurate separation between irrigated and rainfed cropland can be made with the LGRIP30 v001 dataset (Teluguntla et al., 2023). LGRIP data are produced using Landsat 8 time-series satellite sensor data for the 2014-2017 time period, from which a nominal 2015 product is created. Since a very small part of the land cover changed over the years (0.79 %), no large deviations are expected to arise by using this nominal product. The dataset's spatial resolution of 30 meters ensures an accurate differentiation between irrigated and rainfed cropland. Appendix figure 14 shows the LGRIP30 v001 dataset for the study area. Large parts of Nebraska are classified as irrigated cropland, in contrast to ESA CCI land cover dataset (Copernicus Climate Change Service, 2019) where everything was classified as rainfed cropland. Due to the high spatial resolution and the corresponding extended calculation time, the analysis was limited to a small area at the border between Nebraska and Colorado, highlighted in Appendix figure 14. The results of this analysis are displayed in Appendix figures 15 and 16. Due to the small spatial scale of the area, data was not present in all classes of drought time and intensity. Consequently, the results may not be entirely reliable, potentially exhibiting a different trend over a larger geographical area. In this small area differences between irrigated and rainfed cropland arise, the average vegetation recovery time for irrigated cropland in figure 15b (calculated with the 'first method', mentioned in section 2.4) is 151 days and remains relatively equal over all drought lengths. The average vegetation recovery time for rainfed cropland in figure 16b is 171 days and shows a slight increase with increasing drought lengths. The difference between the regeneration time of these two crop types is probably caused by irrigation. Future research could expand the performed analysis by combining the land cover datasets. If data is identified as cropland (all types) by the ESA CCI land cover, the LGRIP30 v001 dataset can differentiate between irrigated and rainfed cropland. It would be intriguing to investigate whether the slight differences that seem to arise between the two crop types also hold for larger spatial areas. So, large-scale hydrological models like PCR-GLOBWB 2.0 (Sutanudjaja et al., 2018) can be im-

proved through the estimation of crop water requirements for both irrigated and rainfed crops across various drought lengths and intensities during the recovery period.

4.2 Spatial patterns of vegetation recovery

Highest correlation coefficients are found for grassland at modest altitudes in the center of the study area. Further to the northwest where the altitude increases the correlation coefficient is slightly lower. This worsening correlation is induced by climatic conditions. In the study area, winters can be dominated by snowy conditions, especially at higher altitudes (Fassnacht et al., 2016). This snow coverage can interfere with the correlation between SPEI and EVI as the vegetation greenness can not be accurately measured. During a drought, there is less precipitation or higher evapotranspiration rates than normal. Less or no snow will then be expected, even at higher altitudes (Bathke et al., 2014). Consequently, the correlation coefficient in figure 6a is also high (almost 1.0) at elevated altitudes. These higher values, however, are somewhat less reliable as the cross-correlation is performed over a selected time period. The cross-correlation in figure 5 is performed over the entire time series of 414 data points. While in figure 6 the cross-correlation can be limited to only a few data points. This shorter time series can make the cross-correlation less significant, making it easier for uncertainties to arise.

These uncertainties are also visible in figure 6b. The time shift does not show a clear distribution over the study area. While the time shift in figure 5b showed lower time shifts further from the North Platte River. This is due to the hydraulic gradient in the area. The river causes a low hydraulic head in the region, so most groundwater flows towards this stream. Therefore, the water table in the river valley is high. But the elevation quickly increases from the river valley towards the Great Plains. This creates a larger unsaturated zone at the slopes near the river valley, visible with the Real-Time Groundwater Monitoring Network of the University of Nebraska–Lincoln (UNL, 2023). The water table in the monitoring well at the slope next to the North Platte River is on average 60 feet below the land surface. While monitoring wells on the Great Plains show the water table is between 1 and 20 feet below the surface. The larger unsaturated zone is a disadvantage for vegetation because they have to root deeper to reach the water table (Fan et al., 2017). At the Great Plains, the elevation does not show these steep differences. Hence, the water table in this area is closer to the surface, allowing vegetation roots to access water without the need to extend as deeply. The thicker unsaturated (or vadose) zone, also causes a groundwater recharge delay (Wossenyeleh et al., 2020). Groundwater flow in the vadose zone is driven by gravity, which means the water flows vertically through this zone to recharge groundwater. The thicker the vadose zone the longer it takes for precipitation to reach the groundwater table and therefore causes a delayed response. During a severe drought, there is a prolonged period of precipitation reduction. The thick vadose zone causes a delayed response in the groundwater table, which means it decreases later in the drought. The moment precipitation returns to mean values the groundwater table keeps decreasing as precipitation first needs to flow through the thick vadose zone. This causes the groundwater recharge delay and longer vegetation recovery times in areas with thicker vadose zones. This is supported by the study of Rossman et al. (2014), which estimated the vadose zone lag time in Nebraska. The results show the longest vadose zone lag times in areas with a thick vadose zone. The areas with long vadose zone lag times align with those in this study demonstrating large time shifts, illustrated in figure 5b and mainly figure 6b. Indicating that long vadose zone lag times result in a delayed vegetation response. On top of that, the Great Plains are also a recharge area, the water table is first to increase here after a drought. Climate change will enhance the effect because more precipitation will fall as rain instead of snow, increasing the recharge rates in the area (Crosbie et al., 2013). The combination of the water table, rooting depth, groundwater recharge delay and the recharge area causes the time shift, the time it takes for the EVI to respond on the SPEI, to be shorter further from the North Platte River. The difference in time

shift is quite significant, as on average near the river it is 125 days, and deeper onto the Great Plains it is towards 75 days.

Another factor that may contribute to the vegetation regeneration time, and cause the more scattered distribution of the time shift in figure 6b, can potentially be explained by taking a closer look at the land cover of Nebraska. Figure 1 shows a lot of blue patches in the grassland, these are naturally formed local depressions filled with water. In the regions with lots of these depressions, there is no or a very low time shift (below 50 days). In regions where these depressions are not present in the grassland, the time shift can go up to 150 days. Therefore it is likely the vegetation is using these local depressions filled with water to limit the drought impact. While the areas without availability to water, logically are more affected and need more time to recover from droughts. The different recovery times of the vegetation can also be caused due to a difference in the response time to first recharge by precipitation. For both a low and high time shift in the grassland the time series for soil moisture are reviewed, these are shown in Appendix figures 17 and 18. The soil moisture for the location with a low time shift (figure 18) seems to be less responsive to droughts than the location with a high time shift (figure 17). This can be due to the naturally formed local depressions or due to an unavailability of data, explained in section 2.3. On the contrary, the soil moisture in figure 18 recovers slower after the 2012/2013 drought than in figure 17. This would indicate a shorter vegetation recovery time in figure 17 than in figure 18. This contradiction ensures that pinpointing an exact reason for the vegetation recovery time remains elusive, preventing a definitive conclusion as to what causes the difference in this region.

The illogical correlation and time shifts in the southeast corner of the study area (figure 6) are caused by spatial differences between the datasets. In this case, the SPEI is the cause of the deviating values. The large spatial resolution is visible in the area compared to the smaller resolution of the EVI. The bad correlation values are sharply cut from the surrounding regions. As only droughts are selected and the same deviations are not visible in figure 5, it means that the SPEI deviates at this location only during the droughts and vegetation recovery. A smaller spatial resolution of the data could potentially resolve this problem. The transition between areas will be smoother and the SPEI can be determined more accurately for the area.

Decreasing the spatial resolution also has a downside, as it costs more time to process all the data. Already, the study area was limited in size due to the large processing and calculation time. Parallelization is a possible solution to reduce the computational time for the performed calculations. By parallel processing, tasks are distributed across multiple cores or processors. The computational time can be decreased to 10% of the original time (Samuel, 2012). This is a significant decrease which makes it easier to process larger areas of interest. When the computational time is reduced, it would be useful to spatially upscale this research to larger areas. First to several states in the U.S. or even to the entire U.S., to compare the vegetation regeneration time between different regions and climatic zones. It can even be compared to different regions across the world, such as the Rhine Meuse basin, to assess the validity of these relationships. The advantage of this is that the results become more significant and relations can be applied to larger areas rather than being limited to the study area. But, the upscaling has to be done without losing sight of the regional characteristics. In the study area used in this research significant differences already occurred, while this is geomorphological not a challenging area.

4.3 Assess recovery time based on drought separation

The length of the negative vegetation anomalies shows almost a linear trend between 0 and 300 days (figure 7a). For every class, the vegetation recovery increases with approximately 25 days as the drought time increases with 50 days, until it remains stable around a recovery time of 350 days. Similarly, the drought intensity increases linearly between -0.75/-1.0 and -1.25/-1.5 with 60 days per class (figure 7d). Also, in this figure it remains stable around the recovery time of 350 days. This shows that the drought time and intensity certainly have an impact on the grassland. But from some intensity and drought length, the impact on the vegetation remains the same as it does not stay longer than 350 days below the -SD, even for droughts that take longer. In the figures 7b and e, the vegetation recovery is calculated by the 'first method' (section 2.4). Where it continually moves around the mean of 121 days for all the different drought lengths and intensities. This means the vegetation regeneration time is not dominated by drought characteristics. In the study of Yao et al. (2023) soil moisture was found as the dominant factor for recovery time. Currently, soil moisture dominates the drought recovery time of almost 60% of the assessed land worldwide. Due to the acceleration and intensification of drought events, soil moisture is expected to decline in over 65% of the regions worldwide in the future. This will lead to longer drought recovery times and exacerbate the effects of droughts on vegetation. Also, in this research soil moisture dominates the recovery time. It does not matter how intense the drought was, the recovery time always stays around 121 days. But it can deviate between 10 and 300 days dependent on the soil moisture content during the recovery period.

In figure 7c and f the recovery time declines the longer or more intense a drought becomes. This is due to a limitation in the method ('second method', mentioned in section 2.4) used to calculate the recovery time. Generally, the longer a drought lasts the more intense it is (Appendix figure 11). This also means for longer droughts the impact on the vegetation already becomes visible during the drought, despite the delayed response between these two (figure 5b). Severe and extreme droughts take more time to return to normal conditions or in this case the -0.5 threshold. In this time conditions improve, the drought becomes less severe, and vegetation can already start to recover. By the time the drought reaches the threshold of -0.5, the vegetation already had time to recover. Therefore, moderate droughts which have a delayed vegetation response outside the drought, show a longer recovery time than severe droughts.

By decreasing the threshold for droughts to -1.0, drought times decrease. As drought times decrease, vegetation has less time to recover within the drought and the problem in the calculation of the 'second method' should become less pronounced. Appendix figure 13 shows the vegetation recovery times of grassland with a decreased threshold. As expected the general regeneration time increases to 125 days now mild droughts are excluded from the analysis. Figure 13c and f still show decreasing vegetation regeneration times for increasing drought times, which matches the trend observed in figure 7c and f. The desired effect has not been achieved by decreasing the threshold, the limitation in the 'second method' remains and the vegetation recovery time still decreases for longer drought times. By decreasing the threshold for droughts also the conditions set in section 2.4 should be revised. By decreasing the threshold the drought(s) with an intensity between -2.25 and -2.5 did not meet the requirements and is therefore excluded from the analysis.

However, the mean regeneration time for grassland in figure 7 does not differ much between the two methods, 121 and 135 days respectively. Other studies that investigated the recovery time found varying results. Anderegg et al. (2015) found a recovery time of 1-4 years from severe droughts by examining tree rings. Schwalm et al. (2017) calculated that in 75% of the cases where vegetation recovers after a drought, it takes less than 6 months. But in the last decades longer recovery times become more frequent and can even reach 24 months. Yu et al. (2017) found a recovery time of $\sim$ 80 days for grassland. By using the MODIS DSI product to detect

drought occurrences and determine the recovery from the Ecosystem GPP. He et al. (2018) also used the GPP to determine the ecosystem recovery and found a recovery time between 21 and 36 days. But in the latest study of Yao et al. (2023) the same method is implemented as in this research. Only different vegetation indexes are used, they used LAI, kNDVI and SIF whereas in this research EVI is used. When the recovery time was calculated with the 'first method' (section 2.4) the recovery time was 3.11, 3.22 and 3.05 months respectively. That is close to the average recovery times found in this research, 3.97 months (121 days) for grassland and 3.64 months (111 days) for cropland.

The vegetation recovery classified by drought timing (figure 9) exhibits a discernible pattern for both grassland and cropland. For grassland the recovery time increases till the month of October. When a drought ends in this month it needs the most time to recover to a pre-drought state. This corresponds to the growing season of natural vegetation in the northern hemisphere, here the growing season begins in late April-early May and ends late September-early October (Volesky et al., 2005). When a drought ends in October the growing season is over and no favorable conditions are met for the recovery of vegetation. Vegetation has to wait till the beginning of the growing season to recover. This is the difference between the regeneration time of April and October, 100 days vs 220 days. The time between the end and beginning of the growing season is 5 months (150 days). Therefore, the later a drought ends in the growing season the more time vegetation needs to recover. The severity of the drought when it ends in September or October can influence the regeneration time strongly. Regeneration times can increase to 600 days if a severe drought ends in these months.

Cropland shows a slightly different vegetation recovery in relation to drought timing. Here the peak of the regeneration time is already reached in July. This again corresponds to the growing season of in this case cropland. Most crops are grown from late spring (May) and need at least 80 days to grow (Kukal and Irmak, 2018). From April a steep increase in regeneration time is visible till it reaches its peak in July. When a drought ends in this month it has the longest regeneration time as the growing season is over. From this moment it has to wait till May of next year before crops are grown there again, therefore the regeneration time is exactly 300 days (10 months). Also, here the severity of the drought plays an important role. In some cases the regeneration time goes up to 700 days, meaning a year after the drought hit the area the ecosystem was not recovered enough to grow crops. Again, soil moisture plays an important role in the length of these regeneration times. As crops are not as deeply rooted as natural vegetation, they are highly dependent on the soil moisture in the topsoil (Holzman et al., 2014). If this is not properly recharged after a drought, crops can not grow in the area.

The outliers of March and May are present in both grassland and cropland. Meaning the deviations in the data are not limited to land cover classes and therefore occurred over the entire study area. There are multiple possible explanations for these deviations. The first one is that the drought frequency played a role in the regeneration time (Jiao et al., 2021). If two droughts followed in short succession, the vegetation did not have time to recover in between. This can eventually lead to a longer recovery time after the second drought. The second explanation can be that the droughts ended in March or May lasted long or were quite intense. In combination with a disproportionate sampling frequency over the months, deviations may occur. An under-sampling is indeed visible in March (Appendix figure 12). Only in 0.02% (n = 0.0002) of the pixels a drought did end in this month, almost all of which correspond to one drought. This drought is relatively short and moderate but shows large variations in recovery time. As these deviations are observed in both grassland and cropland, it suggests potential minor inaccuracies in the EVI time series or vegetation was not yet recovered from a previous drought, resulting in above-average regeneration times. The month of May is not under-sampled (n = 0.05) compared to the other months, therefore the most logical explanation for the deviation in the vegetation

regeneration time here is the drought frequency. Vegetation took longer than average to recover from two or multiple consecutive droughts in the month of May.

5 Conclusion

In this study, a coupling is defined between the drought index and vegetation regeneration in Nebraska, United States. To properly assess varied responses to drought events and their subsequent impacts on vegetation regeneration times, a difference is made between grassland and cropland. Results show a clear link between land cover types and their response to droughts, correlation coefficients are usually much higher for grassland (0.5 - 1.0) than cropland (0.0 - 0.4). Especially in the central part of Nebraska where the Great Plains begin, grassland exhibited higher correlation coefficients, emphasizing its vulnerability and responsiveness to drought events. Cropland, influenced by anthropogenic factors like irrigation and crop cultivation, displayed no correlation patterns. Hence, it becomes important to distinguish between rainfed and irrigated cropland in future studies. This can be achieved by combining the ESA CCI land cover and the LGRIP30 v001 dataset. Preliminary testing of the analysis using the LGRIP30 v001 dataset over a limited spatial area yielded promising results. Consequently, further improvement of the analysis with this dataset could offer a more comprehensive understanding of the divergent responses between rainfed and irrigated cropland in future studies. The time shifts, the time it takes for the EVI to respond to the SPEI, for grassland follows certain spatial patterns that are induced by local topography which is the main driver of groundwater flow and therefore hydraulic gradients in the area. Various other factors, including the water table, rooting depth, groundwater recharge delay, recharge area, local depressions filled with water, as well as soil moisture, contribute to deviations in time shifts and recovery times within the study area. Vegetation regeneration time for grassland remains around 121 days for all the different drought lengths and intensities. So, droughts are not the dominant component in vegetation recovery, soil moisture is. Recovery time for cropland has a capricious pattern, due to a mixture of rainfed and irrigated cropland in the data. Nevertheless, the average recovery time is close to that of grassland, as it is 111 days. Although drought length and intensity do not play a dominant role in vegetation recovery, drought timing does. If droughts end late in the growing season, vegetation requires more time to recover. Usually, it takes until the next growing season for it to recover. But when the drought is severe, soil moisture requires more time to recharge and vegetation recovery can take over one year. Emphasizing the importance of considering drought timing and soil moisture in future studies of vegetation recovery. This research contributes to the understanding of vegetation responses to drought, providing valuable information for large-scale hydrological models such as PCR-GLOBWB 2.0. In the future, soil moisture is projected to decline, our insights underscore the need for accurate estimates of vegetation water demands during post-drought periods. This, in turn, can inform sustainable water resource management strategies, crucial for mitigating the escalating impacts of drought on global ecosystems. Reducing computational time would enhance the feasibility of upscaling this research to larger areas. This would allow for a comprehensive comparison of vegetation regeneration times and the predominant factors controlling them across various regions and climatic zones. Such a comparison could contribute to a more accurate global estimation of water demands during post-drought periods.

References

Anderegg, W. R. L., Schwalm, C., Biondi, F., Camarero, J. J., Koch, G., Litvak, M., Ogle, K., Shaw, J. D., Shevliakova, E., Williams, A. P., Wolf, A., Ziaco, E., and Pacala, S. (2015). Pervasive drought legacies in forest ecosystems and their implications for carbon cycle models. *Science*, 349(6247):528–532. Publisher: American Association for the Advancement of Science.

Bathke, D., Oglesby, R., Rowe, C., and Wilhite, D. (2014). Understanding and Assessing Climate Change: Implications for Nebraska. *Department of Earth and Atmospheric Sciences: Faculty Publications*.

Burke, E. J., Brown, S. J., and Christidis, N. (2006). Modeling the Recent Evolution of Global Drought and Projections for the Twenty-First Century with the Hadley Centre Climate Model. *Journal of Hydrometeorology*, 7(5):1113–1125. Publisher: American Meteorological Society Section: Journal of Hydrometeorology.

Chirouze, J., Boulet, G., Jarlan, L., Fieuzal, R., Rodriguez, J. C., Ezzahar, J., Er-Raki, S., Bigeard, G., Merlin, O., Garatuza-Payan, J., Watts, C., and Chehbouni, G. (2014). Intercomparison of four remote-sensing-based energy balance methods to retrieve surface evapotranspiration and water stress of irrigated fields in semi-arid climate. *Hydrology and Earth System Sciences*, 18(3):1165–1188. Publisher: Copernicus GmbH.

Copernicus Climate Change Service, C. D. S. (2019). Land cover classification gridded maps from 1992 to present derived from satellite observation.

Crosbie, R. S., Scanlon, B. R., Mpelasoka, F. S., Reedy, R. C., Gates, J. B., and Zhang, L. (2013). Potential climate change effects on groundwater recharge in the High Plains Aquifer, USA. *Water Resources Research*, 49(7):3936–3951. _eprint: https://onlinelibrary.wiley.com/doi/pdf/10.1002/wrcr.20292.

Davis, T. W., Prentice, I. C., Stocker, B. D., Thomas, R. T., Whitley, R. J., Wang, H., Evans, B. J., Gallego-Sala, A. V., Sykes, M. T., and Cramer, W. (2017). Simple process-led algorithms for simulating habitats (SPLASH v.1.0): robust indices of radiation, evapotranspiration and plant-available moisture. *Geoscientific Model Development*, 10(2):689–708. Publisher: Copernicus GmbH.

Deb, P., Moradkhani, H., Han, X., Abbaszadeh, P., and Xu, L. (2022). Assessing irrigation mitigating drought impacts on crop yields with an integrated modeling framework. *Journal of Hydrology*, 609:127760.

Delfine, S., Loreto, F., and Alvino, A. (2001). Drought-stress Effects on Physiology, Growth and Biomass Production of Rainfed and Irrigated Bell Pepper Plants in the Mediterranean Region. *Journal of the American Society for Horticultural Science*, 126(3):297–304. Publisher: American Society for Horticultural Science Section: Journal of the American Society for Horticultural Science.

Didan, K. (2015). MYD13C1 MODIS/Aqua Vegetation Indices 16-Day L3 Global 0.05Deg CMG V006. NASA EOSDIS Land Processes Distributed Active Archive Center.

Dorigo, W., Preimesberger, W., Hahn, S., Van der Schalie, R., De Jeu, R., Kidd, R., Rodriguez-Fernandez, N., Hirschi, M., Stradiotti, P., Frederikse, T., Gruber, A., and Madelon, R. (2023). ESA Soil Moisture Climate Change Initiative (Soil_moisture_cci): ACTIVE product, Version 08.1.

Dutta, D., Kundu, A., Patel, N. R., Saha, S. K., and Siddiqui, A. R. (2015). Assessment of agricultural drought in Rajasthan (India) using remote sensing derived Vegetation Condition Index (VCI) and Standardized Precipitation Index (SPI). *The Egyptian Journal of Remote Sensing and Space Science*, 18(1):53–63.

Elmore, A. J., Manning, S. J., Mustard, J. F., and Craine, J. M. (2006). Decline in alkali meadow vegetation cover in California: the effects of groundwater extraction and drought. *Journal of Applied Ecology*, 43(4):770–779. _eprint: https://onlinelibrary.wiley.com/doi/pdf/10.1111/j.1365-2664.2006.01197.x.

Fan, Y., Miguez-Macho, G., Jobbágy, E. G., Jackson, R. B., and Otero-Casal, C. (2017). Hydrologic regulation of plant rooting depth. *Proceedings of the National Academy of Sciences*, 114(40):10572–10577. Publisher: Proceedings of the National Academy of Sciences.

Fassnacht, S. R., Cherry, M. L., Venable, N. B. H., and Saavedra, F. (2016). Snow and albedo climate change impacts across the United States Northern Great Plains. *The Cryosphere*, 10(1):329–339. Publisher: Copernicus GmbH.

Fathi-Taperasht, A., Shafizadeh-Moghadam, H., Minaei, M., and Xu, T. (2022). Influence of drought duration and severity on drought recovery period for different land cover types: evaluation using MODIS-based indices. *Ecological Indicators*, 141:109146.

Fontana, D., Potgieter, A., and Apan, A. (2007). Assessing the relationship between shire winter crop yield and seasonal variability of the MODIS NDVI and EVI images. *Applied GIS*, 3.

He, B., Liu, J., Guo, L., Wu, X., Xie, X., Zhang, Y., Chen, C., Zhong, Z., and Chen, Z. (2018). Recovery of Ecosystem Carbon and Energy Fluxes From the 2003 Drought in Europe and the 2012 Drought in the United States. *Geophysical Research Letters*, 45(10):4879–4888. _eprint: https://onlinelibrary.wiley.com/doi/pdf/10.1029/2018GL077518.

Holzman, M. E., Rivas, R., and Piccolo, M. C. (2014). Estimating soil moisture and the relationship with crop yield using surface temperature and vegetation index. *International Journal of Applied Earth Observation and Geoinformation*, 28:181–192.

Huang, K., Yi, C., Wu, D., Zhou, T., Zhao, X., Blanford, W. J., Wei, S., Wu, H., Ling, D., and Li, Z. (2015). Tipping point of a conifer forest ecosystem under severe drought. *Environmental Research Letters*, 10(2):024011. Publisher: IOP Publishing.

Jiao, T., Williams, C. A., De Kauwe, M. G., Schwalm, C. R., and Medlyn, B. E. (2021). Patterns of post-drought recovery are strongly influenced by drought duration, frequency, post-drought wetness, and bioclimatic setting. *Global Change Biology*, 27(19):4630–4643. _eprint: https://onlinelibrary.wiley.com/doi/pdf/10.1111/gcb.15788.

Joo, E., Zeri, M., Hussain, M. Z., DeLucia, E. H., and Bernacchi, C. J. (2017). Enhanced evapotranspiration was observed during extreme drought from Miscanthus, opposite of other crops. *GCB Bioenergy*, 9(8):1306–1319. _eprint: https://onlinelibrary.wiley.com/doi/pdf/10.1111/gcbb.12448.

Keyantash, J. and Dracup, J. A. (2002). The Quantification of Drought: An Evaluation of Drought Indices. *Bulletin of the American Meteorological Society*, 83(8):1167–1180. Publisher: American Meteorological Society Section: Bulletin of the American Meteorological Society.

Konikow, L. F. and Kendy, E. (2005). Groundwater depletion: A global problem. *Hydrogeology Journal*, 13(1):317–320.

Kukal, M. S. and Irmak, S. (2018). U.S. Agro-Climate in 20th Century: Growing Degree Days, First and Last Frost, Growing Season Length, and Impacts on Crop Yields. *Scientific Reports*, 8(1):6977. Number: 1 Publisher: Nature Publishing Group.

Lal, R., Delgado, J. A., Gulliford, J., Nielsen, D., Rice, C. W., and Pelt, R. S. V. (2012). Adapting agriculture to drought and extreme events. *Journal of Soil and Water Conservation*, 67(6):162A–166A. Publisher: Soil and Water Conservation Society Section: A Section.

Lesk, C., Rowhani, P., and Ramankutty, N. (2016). Influence of extreme weather disasters on global crop production. *Nature*, 529(7584):84–87. Number: 7584 Publisher: Nature Publishing Group.

Li, Y., Ye, W., Wang, M., and Yan, X. (2009). Climate change and drought: a risk assessment of crop-yield impacts. *Climate Research*, 39(1):31–46.

Li, Y., Zhang, W., Schwalm, C. R., Gentine, P., Smith, W. K., Ciais, P., Kimball, J. S., Gazol, A., Kannenberg, S. A., Chen, A., Piao, S., Liu, H., Chen, D., and Wu, X. (2023). Widespread spring phenology effects on drought recovery of Northern Hemisphere ecosystems. *Nature Climate Change*, 13(2):182–188. Number: 2 Publisher: Nature Publishing Group.

Liu, L., Gudmundsson, L., Hauser, M., Qin, D., Li, S., and Seneviratne, S. I. (2019). Revisiting assessments of ecosystem drought recovery. *Environmental Research Letters*, 14(11):114028. Publisher: IOP Publishing.

Lopez-Nicolas, A., Pulido-Velazquez, M., and Macian-Sorribes, H. (2017). Economic risk assessment of drought impacts on irrigated agriculture. *Journal of Hydrology*, 550:580–589.

Lu, J., Carbone, G. J., Huang, X., Lackstrom, K., and Gao, P. (2020). Mapping the sensitivity of agriculture to drought and estimating the effect of irrigation in the United States, 1950–2016. *Agricultural and Forest Meteorology*, 292-293:108124.

McKee, T. B., Doesken, N. J., and Kleist, J. (1993). THE RELATIONSHIP OF DROUGHT FREQUENCY AND DURATION TO TIME SCALES. *8th Conference on Applied Climatology*.

Müller, L. M. and Bahn, M. (2022). Drought legacies and ecosystem responses to subsequent drought. *Global Change Biology*, 28(17):5086–5103. _eprint: https://onlinelibrary.wiley.com/doi/pdf/10.1111/gcb.16270.

NeDNR (2023). Platte River Conjunctive Management Study | Department of Natural Resources.

Palmer, W. C. (1965). *Meteorological Drought*. U.S. Department of Commerce, Weather Bureau.

Potop, V., Možný, M., and Soukup, J. (2012). Drought evolution at various time scales in the lowland regions and their impact on vegetable crops in the Czech Republic. *Agricultural and Forest Meteorology*, 156:121–133.

Potopová, V., Boroneanţ, C., Boincean, B., and Soukup, J. (2016). Impact of agricultural drought on main crop yields in the Republic of Moldova. *International Journal of Climatology*, 36(4):2063–2082. _eprint: https://onlinelibrary.wiley.com/doi/pdf/10.1002/joc.4481.

Ray, R. L., Fares, A., and Risch, E. (2018). Effects of Drought on Crop Production and Cropping Areas in Texas. *Agricultural & Environmental Letters*, 3(1):170037. _eprint: https://onlinelibrary.wiley.com/doi/pdf/10.2134/ael2017.11.0037.

Rippey, B. R. (2015). The U.S. drought of 2012. *Weather and Climate Extremes*, 10:57–64.

Rossman, N. R., Zlotnik, V. A., Rowe, C. M., and Szilagyi, J. (2014). Vadose zone lag time and potential 21st century climate change effects on spatially distributed groundwater recharge in the semi-arid Nebraska Sand Hills. *Journal of Hydrology*, 519:656–669.

Samuel, H. (2012). Time domain parallelization for computational geodynamics. *Geochemistry, Geophysics, Geosystems*, 13(1). _eprint: https://onlinelibrary.wiley.com/doi/pdf/10.1029/2011GC003905.

Schwalm, C. R., Anderegg, W. R. L., Michalak, A. M., Fisher, J. B., Biondi, F., Koch, G., Litvak, M., Ogle, K., Shaw, J. D., Wolf, A., Huntzinger, D. N., Schaefer, K., Cook, R., Wei, Y., Fang, Y., Hayes, D., Huang, M., Jain, A., and Tian, H. (2017). Global patterns of drought recovery. *Nature*, 548(7666):202–205. Number: 7666 Publisher: Nature Publishing Group.

Sutanudjaja, E. H., van Beek, R., Wanders, N., Wada, Y., Bosmans, J. H. C., Drost, N., van der Ent, R. J., de Graaf, I. E. M., Hoch, J. M., de Jong, K., Karssenberg, D., López López, P., Peßenteiner, S., Schmitz, O., Straatsma, M. W., Vannametee, E., Wisser, D., and Bierkens, M. F. P. (2018). PCR-GLOBWB 2: a 5 arcmin global hydrological and water resources model. *Geoscientific Model Development*, 11(6):2429–2453. Publisher: Copernicus GmbH.

Teluguntla, P., Thenkabail, P., Oliphant, A., Gumma, M., Aneece, I., Foley, D., and McCormick, R. (2023). Landsat-Derived Global Rainfed and Irrigated-Cropland Product 30 m V001.

Trenberth, K. E. (2008). The Impact of Climate Change and Variability on Heavy Precipitation, Floods, and Droughts. In *Encyclopedia of Hydrological Sciences*. John Wiley & Sons, Ltd. _eprint: https://onlinelibrary.wiley.com/doi/pdf/10.1002/0470848944.hsa211.

Tsur, Y. (2005). Economic Aspects of Irrigation Water Pricing. *Canadian Water Resources Journal*, 30(1):31–46.

UNL (2023). Real Time Groundwater Levels | Groundwater | Water | Data | School of Natural Resources | Nebraska.

USDA (2022). USDA ERS - Irrigation & Water Use.

Vicente-Serrano, S. M., Beguería, S., and López-Moreno, J. I. (2010). A Multiscalar Drought Index Sensitive to Global Warming: The Standardized Precipitation Evapotranspiration Index. *Journal of Climate*, 23(7):1696–1718. Publisher: American Meteorological Society Section: Journal of Climate.

Volesky, J. D., Schacht, W. H., Reece, P. E., and Vaughn, T. J. (2005). Spring Growth and Use of Cool-Season Graminoids in the Nebraska Sandhills. *Rangeland Ecology & Management*, 58(4):385–392.

Vörösmarty, C. J., Green, P., Salisbury, J., and Lammers, R. B. (2000). Global Water Resources: Vulnerability from Climate Change and Population Growth. *Science*, 289(5477):284–288. Publisher: American Association for the Advancement of Science.

Wang, Q., Wu, J., Lei, T., He, B., Wu, Z., Liu, M., Mo, X., Geng, G., Li, X., Zhou, H., and Liu, D. (2014). Temporal-spatial characteristics of severe drought events and their impact on agriculture on a global scale. *Quaternary International*, 349:10–21.

Wang, S.-Y., Yoon, J.-H., Gillies, R. R., and Cho, C. (2013). What Caused the Winter Drought in Western Nepal during Recent Years? *Journal of Climate*, 26(21):8241–8256. Publisher: American Meteorological Society Section: Journal of Climate.

Wossenyeleh, B. K., Verbeiren, B., Diels, J., and Huysmans, M. (2020). Vadose Zone Lag Time Effect on Groundwater Drought in a Temperate Climate. *Water*, 12(8):2123. Number: 8 Publisher: Multidisciplinary Digital Publishing Institute.

Xu, T., Wu, X., Tian, Y., Li, Y., Zhang, W., and Zhang, C. (2021). Soil Property Plays a Vital Role in Vegetation Drought Recovery in Karst Region of Southwest China. *Journal of Geophysical Research: Biogeosciences*, 126(12):e2021JG006544. _eprint: https://onlinelibrary.wiley.com/doi/pdf/10.1029/2021JG006544.

Yao, Y., Fu, B., Liu, Y., Li, Y., Wang, S., Zhan, T., Wang, Y., and Gao, D. (2022). Evaluation of ecosystem resilience to drought based on drought intensity and recovery time. *Agricultural and Forest Meteorology*, 314:108809.

Yao, Y., Liu, Y., Zhou, S., Song, J., and Fu, B. (2023). Soil moisture determines the recovery time of ecosystems from drought. *Global Change Biology*, 29(13):3562–3574. _eprint: https://onlinelibrary.wiley.com/doi/pdf/10.1111/gcb.16620.

Yu, Z., Wang, J., Liu, S., Rentch, J. S., Sun, P., and Lu, C. (2017). Global gross primary productivity and water use efficiency changes under drought stress. *Environmental Research Letters*, 12(1):014016. Publisher: IOP Publishing.

Zhang, T. and Lin, X. (2016). Assessing future drought impacts on yields based on historical irrigation reaction to drought for four major crops in Kansas. *Science of The Total Environment*, 550:851–860.

6 Appendix

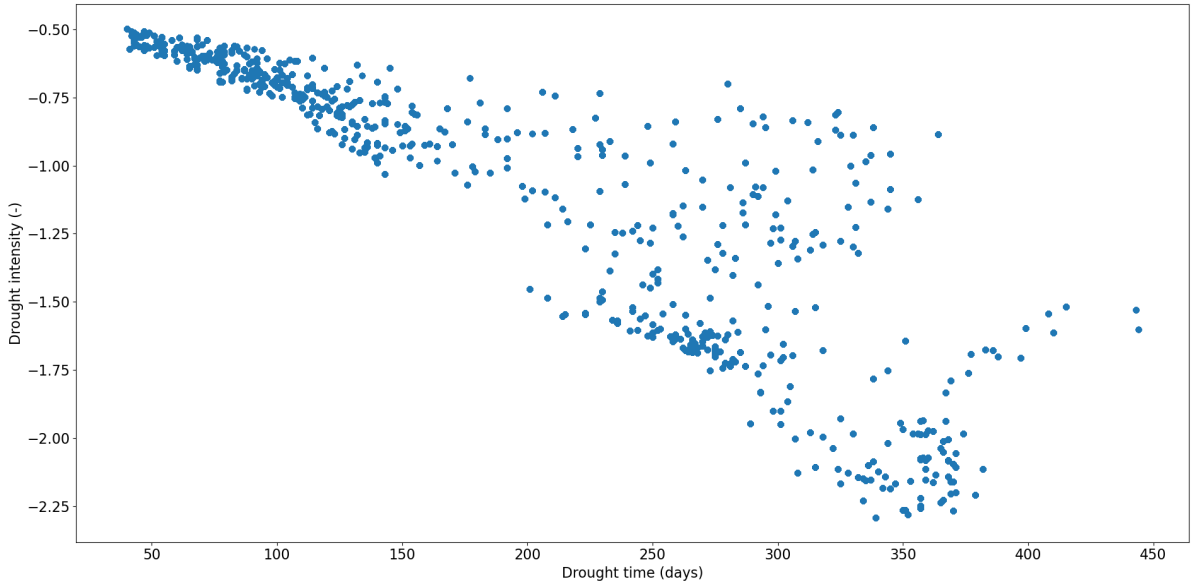

Figure 11: Drought intensity (-) vs drought time (days)

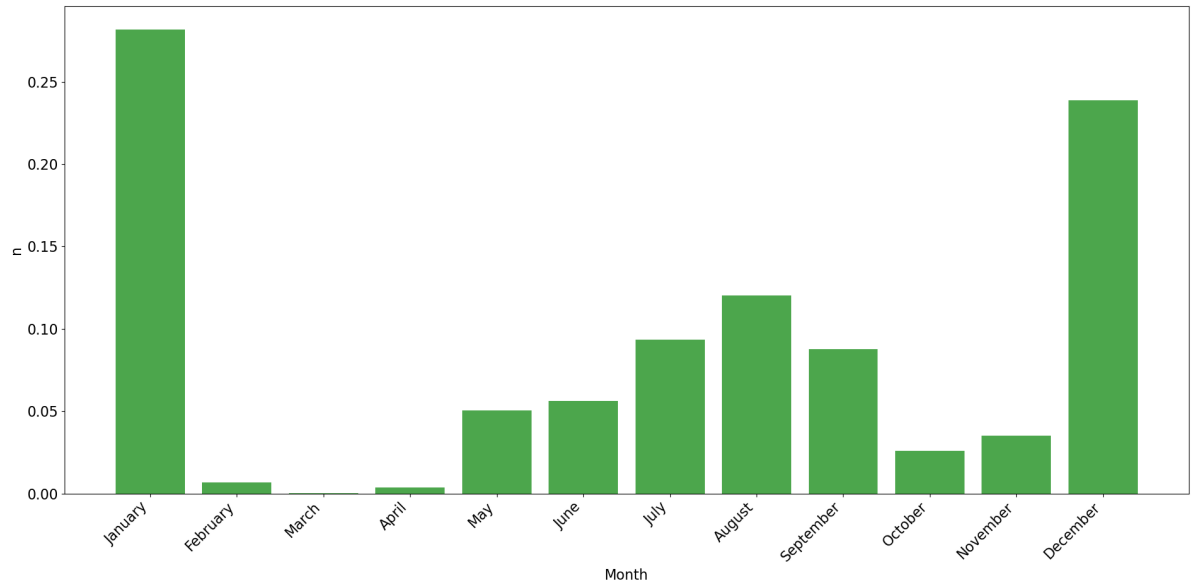

Figure 12: Normalized sampling size (n) of drought timing

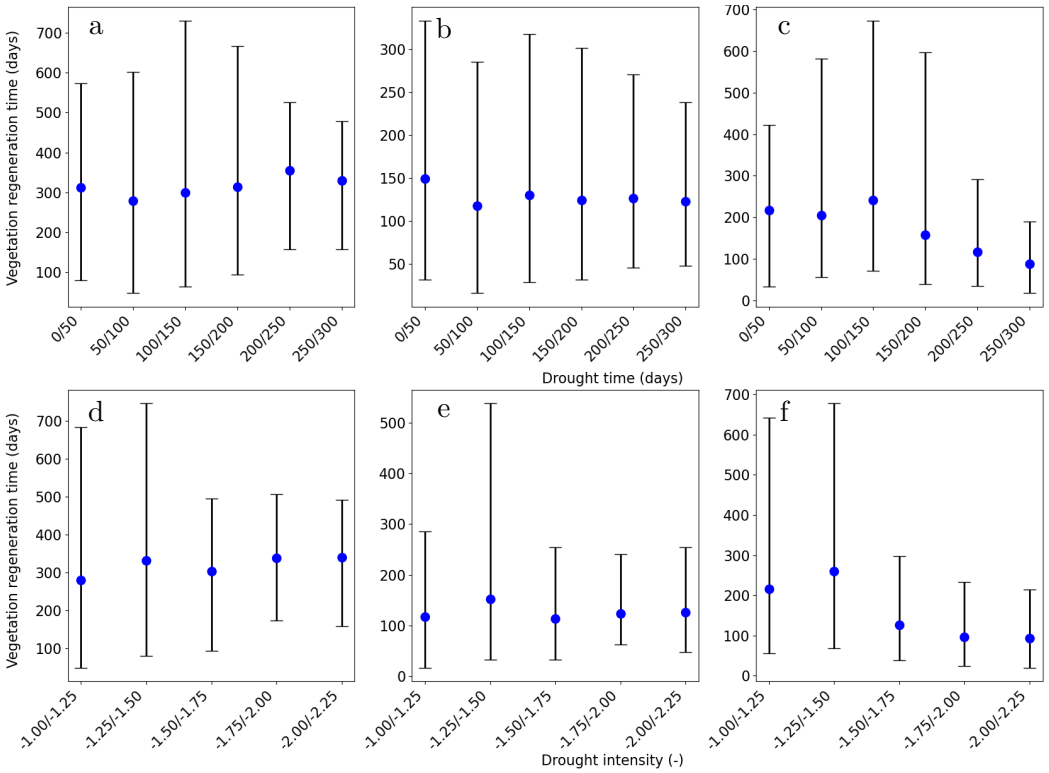

Figure 13: Vegetation recovery of grassland classified by drought length and intensity, with the minimum threshold for droughts set at -1.0. a-c) Recovery time based on drought time. d-f) Recovery time based on drought intensity

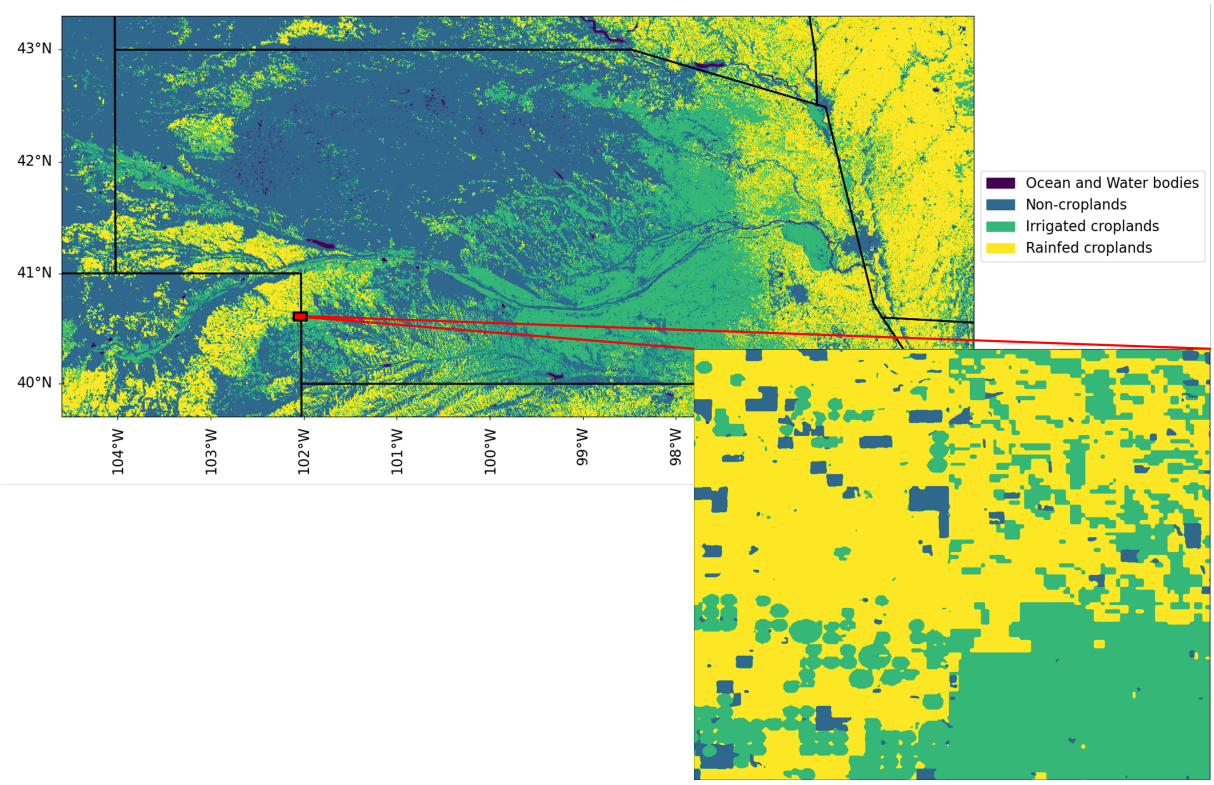

Figure 14: Land cover of Nebraska with accurate separation between irrigated and rainfed cropland. Zoomed area is used for analysis

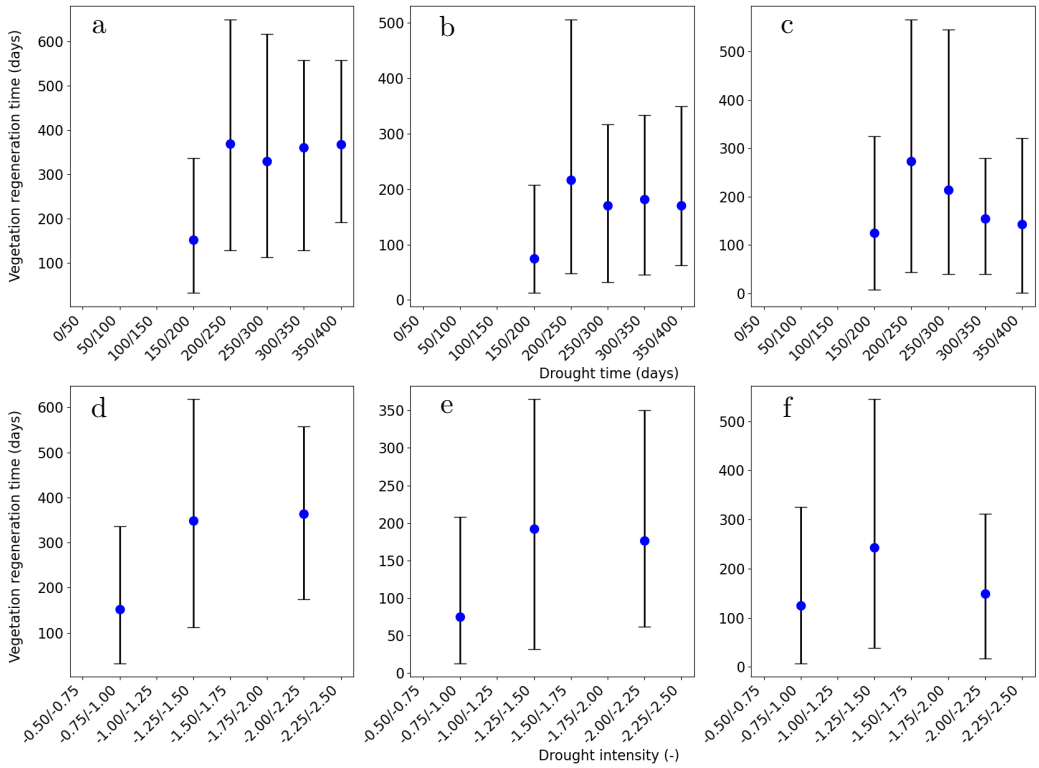

Figure 15: Vegetation recovery of irrigated cropland classified by drought length and intensity based on figure 14. a-c) Recovery time based on drought time. d-f) Recovery time based on drought intensity

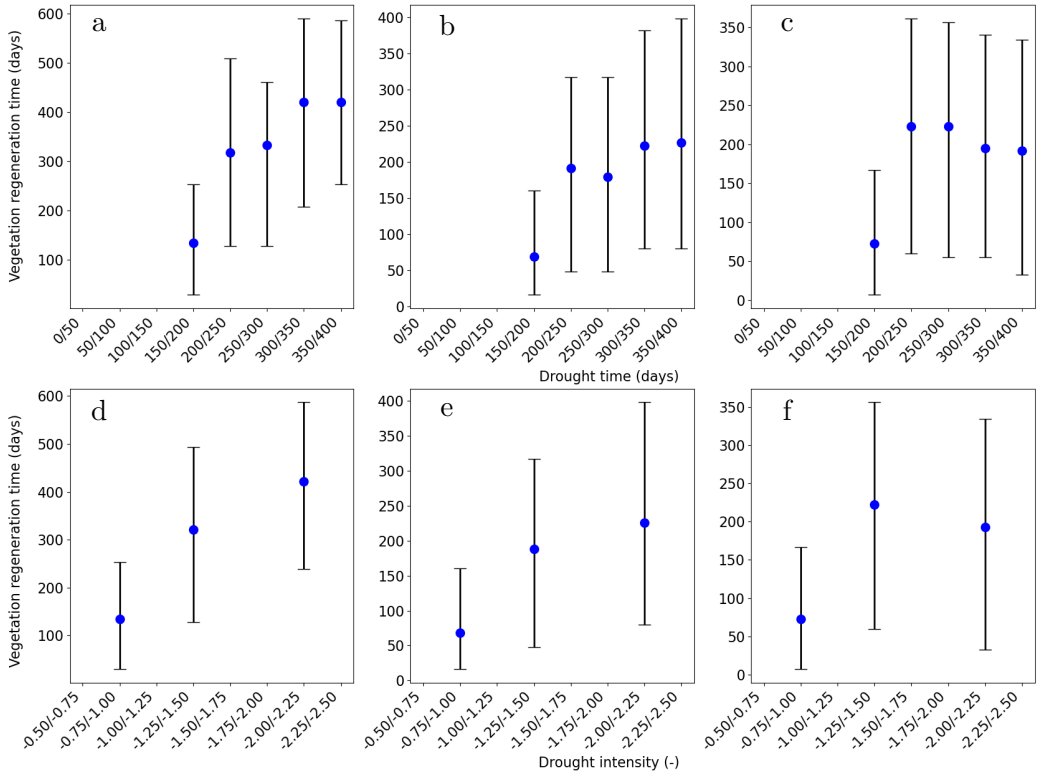

Figure 16: Vegetation recovery of rainfed cropland classified by drought length and intensity based on figure 14. a-c) Recovery time based on drought time. d-f) Recovery time based on drought intensity

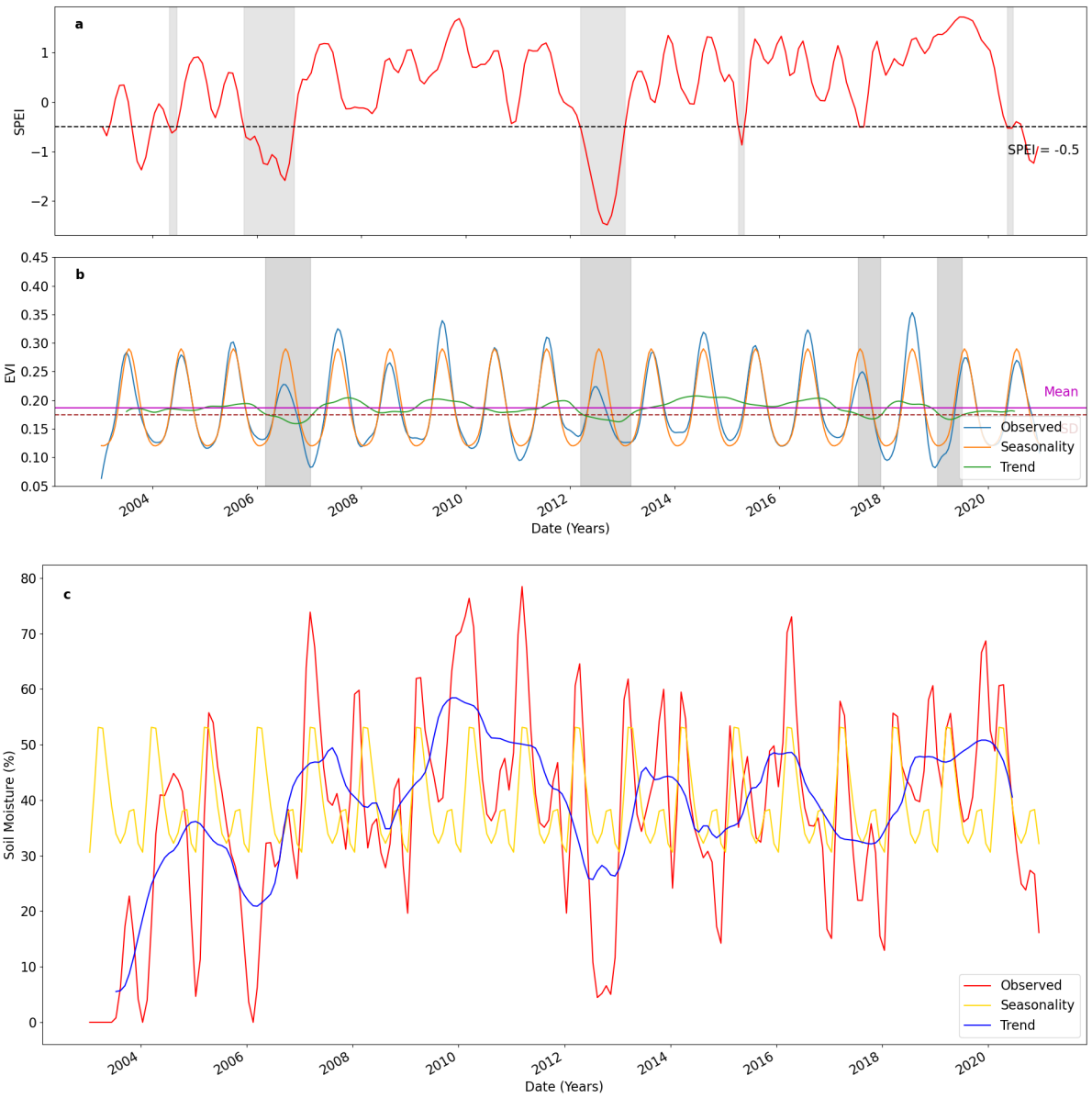

Figure 17: Time series of a)SPEI b)EVI and c)SM at location 41°27'00.0"N 101°03'36.0"W,which corresponds to a high time shift in figure 6b

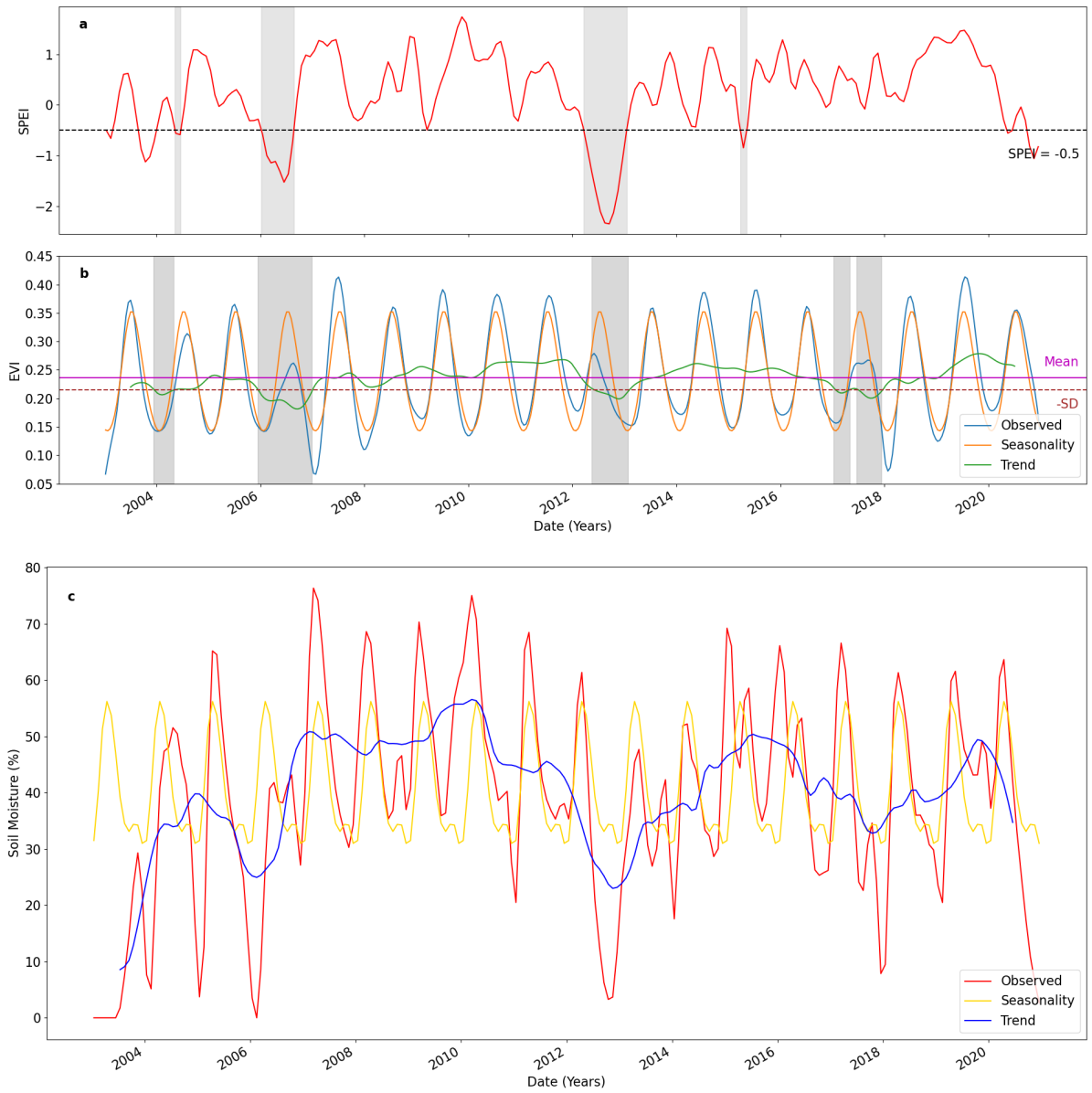

Figure 18: Time series of a)SPEI b)EVI and c)SM at location 42°03'00.0"N 100°36'00.0"W,which corresponds to a low time shift in figure 6b

Land Cover	**Value**
No data	0
Cropland rainfed	10
Cropland rainfed herbaceous cover	11
Cropland rainfed tree or shrub cover	12
Cropland irrigated	20
Mosaic cropland	30
Mosaic natural vegetation	40
Tree broadleaved evergreen closed to open	50
Tree broadleaved deciduous closed to open	60
Tree broadleaved deciduous closed	61
Tree broadleaved deciduous open	62
Tree needleleaved evergreen closed to open	70
Tree needleleaved evergreen closed	71
Tree needleleaved evergreen open	72
Tree needleleaved deciduous closed to open	80
Tree needleleaved deciduous closed	81
Tree needleleaved deciduous open	82
Tree mixed	90
Mosaic tree and shrub	100
Mosaic herbaceous	110
Shrubland	120
Shrubland evergreen	121
Shrubland deciduous	122
Grassland	130
Lichens and mosses	140
Sparse vegetation	150
Sparse tree	151
Sparse shrub	152
Sparce herbaceous	153
Tree cover flooded fresh or brakish water	160
Tree cover flooded saline water	170
Shrub or herbaceous cover flooded	180
Urban	190
Bare areas	200
Bare areas consolidated	201
Bare areas unconsolidated	202
Water	210
Snow and ice	220

Table 1: Land cover classes from UN FAO Land Cover Classification System